FLOW VISUALIZATION OF THE TURBULENT JET AT THE EXIT OF A SINGLE ELEMENT NOZZLE BY HOLOGRAPHIC TECHNIQUE, AND MEAN VELOCITY PROFILE MEASUREMENTS WITH A LASER DOPPLER ANEMOMETER

Ijaz Ahmad Malik

NAVAL POSTGRADUATE SCHOOL
Monterey, California

THESIS

FLOW VISUALIZATION OF THE TURBULENT JET AT THE EXIT OF A SINGLE ELEMENT NOZZLE BY HOLOGRAPHIC TECHNIQUE, AND MEAN VELOCITY PROFILE MEASUREMENTS WITH A LASER DOPPLER ANEMOMETER

by

Ijaz Ahmad Malik

March 1976

Thesis Advisor: D. J. Collins

Approved for public release; distribution unlimited.

REPORT DOCUMENTATION PAGE

READ INSTRUCTIONS BEFORE COMPLETING FORM

1. REPORT NUMBER
2. GOVT ACCESSION NO.
3. RECIPIENT'S CATALOG NUMBER

4. TITLE (and Subtitle)
Flow Visualization of the Turbulent Jet at the Exit of a Single Element Nozzle by Holographic Technique, and Mean Velocity Profile Measurements with a Laser Doppler Anemometer

5. TYPE OF REPORT & PERIOD COVERED
Aeronautical Engineer's Thesis; March 1976

6. PERFORMING ORG. REPORT NUMBER

7. AUTHOR(s)
Ijaz Ahmad Malik

8. CONTRACT OR GRANT NUMBER(s)

9. PERFORMING ORGANIZATION NAME AND ADDRESS
Naval Postgraduate School
Monterey, California 93940

10. PROGRAM ELEMENT, PROJECT, TASK AREA & WORK UNIT NUMBERS

11. CONTROLLING OFFICE NAME AND ADDRESS
Naval Postgraduate School
Monterey, California 93940

12. REPORT DATE
March 1976

13. NUMBER OF PAGES
72

14. MONITORING AGENCY NAME & ADDRESS(if different from Controlling Office)
Naval Postgraduate School
Monterey, California 93940

15. SECURITY CLASS. (of this report)
Unclassified

15a. DECLASSIFICATION/DOWNGRADING SCHEDULE

16. DISTRIBUTION STATEMENT (of this Report)
Approved for public release; distribution unlimited.

17. DISTRIBUTION STATEMENT (of the abstract entered in Block 20, if different from Report)

18. SUPPLEMENTARY NOTES

19. KEY WORDS (Continue on reverse side if necessary and identify by block number)
Holography
Flow Visualization
Turbulent Jet Structure
Turbulent Jet Flow
Single Element Thrust Augmenting Nozzle
Flapping Phenomenon
Laser Doppler Anemometer

20. ABSTRACT (Continue on reverse side if necessary and identify by block number)

The successful application of the holographic technique for flow visualization is reported. The investigation was conducted on the turbulent jet at the exit of a single element oscillating jet nozzle. Both single and double exposure holographic interferograms were employed to determine for an unsteady (oscillating) turbulent jet, the jet structure, spreading rates and the flapping phenomenon. The structure of the steady jet was also investigated for comparison purposes. The mean velocity

20. (continued)

profile measurements of the oscillating and non-oscillating jet were also made with the help of a laser Doppler anemometer and results were compared with the theory and published results obtained by other methods.

FLOW VISUALIZATION OF THE TURBULENT JET AT THE EXIT OF A SINGLE ELEMENT NOZZLE BY HOLOGRAPHIC TECHNIQUE, AND MEAN VELOCITY PROFILE MEASUREMENTS WITH A LASER DOPPLER ANEMOMETER

by

Ijaz Ahmad Malik
Flight Lieutenant, Pakistan Air Force
B.E., Karachi University, 1970

Submitted in partial fulfillment of the
requirements for the degree of

AERONAUTICAL ENGINEER

from the
NAVAL POSTGRADUATE SCHOOL
March 1976

ABSTRACT

The successful application of the holographic technique for flow visualization is reported. The investigation was conducted on the turbulent jet at the exit of a single element oscillating jet nozzle. Both single and double exposure holographic interferograms were employed to determine for an unsteady (oscillating) turbulent jet, the jet structure, spreading rates and the flapping phenomenon. The structure of the steady jet was also investigated for comparison purposes. The mean velocity profile measurements of the oscillating and non-oscillating jet were also made with the help of a laser Doppler anemometer and results were compared with the theory and published results obtained by other methods.

TABLE OF CONTENTS

ACKNOWLEDGEMENTS

The author wishes to gratefully acknowledge Dr.D.J.Collins for his most valuable guidance and assistance in all phases of this investigation; the technical staff of the Department of Aeronautics under R. Besel and T. Dunton, particularly Norman Leckenby and S. Johnson for help in experimental setup; and my wife for her patience and encouragement.

I INTRODUCTION

Holography has opened a new aspect of flow field measurement in aerodynamic research. High power Q-Switched and Dye-Switched lasers and sophisticated double-pulsing trigger mechanisms provide exposure times on the order of twenty nano-seconds, thereby freezing the flow during the hologram production process.

Flow visualization by holography affords certain advantages over other optical techniques due to the unique properties of the holography. It was first determined by Heflinger et al. (Reference 1) that in the case of holography interferometry a far less stringent requirement is placed on the quality of the optical components, namely non-precision optics may be used. Both interfering waves in the case of double exposure holography are equally distorted by the imperfections of the optical parts. This permits interference studies of large objects without high-quality mirrors, windows, and light-dividing plates. The depth focusing capability is another important property of holography which can be useful for examining a specific region of a flow field in detail or to defocus undesirable effects. The angular viewing of the scene is probably the most dramatic effect observed by the unaided eye and this three-dimensionality can be a significant property of a holographic interferogram.

Of the many techniques which have been investigated for holographic flow visualization (References 2,3 and 4),each includes some combination of the following: diffused or direct source illumination, single or double exposure ; and one or two holographic plates. In the double-exposure technique, the first exposure (reference exposure) is usually made with the object at rest and the second exposure is made after the object has been disturbed. ("No flow"-flow

condition in this report). As the object should not move more than one-fifth of the laser's wavelength during each exposure, most experiments in fluid flows require that the exposure time be very short. The pulsed ruby laser is ideal for this purpose since it produces a light pulse having a duration on the order of 20 nano-seconds, which is fast enough to freeze most events. Upon illuminating the hologram, both reference and dynamic scene are reconstructed, resulting in the interference of the two view fields (Reference 5). The interference fringes indicate the areas and degree of dissimilarity between the two states of the same object or flow field. The technique produces a permanent record of the fringe system, which tends to be sharp and of high contrast, thus producing an excellent visual and qualitative view of the field. Use of a singly exposed hologram does not sacrifice the potential of flow field analysis because the hologram stores all of the information regarding the object flow field, and it can be extracted in several ways. The hologram in the case of a fluid flow field is a shadowgraph modulated by the superposition of the reference wave front.The shadowgraph information can be extracted by simply photographing the recorded image using non-coherent light. Schlieren effects are also obtainable with a single exposure. In the case of single exposure holography relatively high quality optics are needed.

In this report the holographic technique is used to study the jet at the exit of a single-element oscillating jet-nozzle in order to indicate visually the enhanced spreading rate and structure of the oscillating jet and also to determine how the jet is flapping from side to side. Holograms of a steady jet were also taken for the comparison of the two cases. Latest studies (Reference 6) indicate that the oscillating jet nozzle may lead to shortening and improvement in the performance of thrust augmenting ejector

devices. In addition, the oscillating nozzles may be of use as fuel injectors on ram-jet configuration and numerous other devices of practical significance.

The second part of this report covers the mean velocity profile measurements of the oscillating and non-oscillating turbulent jet using a laser Doppler anemometer. The major advantages of a laser anamometer are contactless velocity probing and direct digital velocity display, independent of the fluid temperature, pressure and density. The constituent components of the anemometer included a 15 mW laser, an integrated optical unit operating in a fringe mode, a photomultiplier, and a signal processing electronic unit. The flow was seeded with the smoke produced by heating kerosene oil. The mean velocity measurements thus obtained were compared with the theory and with the published results obtained by the other conventional methods.

/

II. HOLOGRAPHIC INVESTIGATION OF THE TURBULENT JET FOR FLOW VISUALISATION

A. EXPERIMENTAL APPARATUS

1. Single element thrust augmenting nozzle

The investigation was conducted on the single element oscillating jet nozzle. The nozzle was built of plexi-glass and was constructed as shown in figures 1 and 2. The throat dimension was 0.25 inches while the width was 2 inches and the separation of the parallel wall diffuser section was 0.406 inches as shown in figure 3.

The two control ports of the bistable fluidic element were connected to each other to cause the jet to oscillate from one side to the other (Reference 6). The basic operation can be shown with the help of figure 4. Consider the jet to be attached to the upper wall A, then , due to the large amount of entrainment into the jet, the pressure at the contrcl port $\acute{A}$ is relatively low while the pressure at the control port $\acute{B}$ is relatively high. Since the ports are attached to each other, a compression wave travels from port $\acute{B}$ to port $\acute{A}$ tending to raise the pressure there and push the jet off the wall; simultaneously , an expansion wave starts at port $\acute{A}$ and travels to port $\acute{B}$, tending to lower the pressure there and pull the jet onto wall B. Thus if the fluidic element is well designed , the jet will separate from wall A and attach to wall B and the process repeats thereafter.

2. The holographic arrangement

The holographic arrangement is illustrated in figure 5 and shown in photographs included as figures 6,7,8 and 9.

Three rigid tables were used as an experimental platform and the nozzle was mounted on a separate stand to avoid nozzle vibration interference. The monochromatic light source used was a KORAD K1QP pulsed ruby laser, operating at a wavelength of 6943 angstroms, together with a dye switch device. The resultant effective exposure time was approximately twenty nano-seconds,eliminating the distortion problem due to the possible nozzle vibration during hologram exposure. A LAUDA constant temperature circulation model K2R was used to maintain the laser head and output etalon at a constant temperature of 27° C.

The scene beam was routed through the nozzle outlet to intersect the reference beam on the holographic plate at an angle. The reference beam was routed through two mirrors, arranged such that reference beam and scene beam path lengths were equal. A diffuser glass mounted on a translation table in the scene beam was used to produce light-field holograms. Alignment of the dye switch laser and system optics was accomplished using a continous wave,low power Helium-Neon laser. To enable hologram production during day time,the experimental set up was arranged in a dark room.

B. EXPERIMENTAL PROCEDURE

1. laboratory technique

The experimental setup shown in figure 5 was used for taking holograms.The coherence length of the source is of great importance in holography.It is necessary that the path difference between any light beams meeting on a hologram not exceed the length of coherence (Reference 7). The coherence length of pulsed ruby laser was approximately ten

centimeters for the output power utilized. This reduced the normally critical requirement for pathlength equality in the scene and reference beams that must be fulfilled in the classical Mach-Zehnder interferometric approach. A length of string proved to be a sufficiently accurate measuring device to maintain the two beam path lengths within the coherence length of the laser.

Lasers emit narrow light beams several millimeters in diameter. Therefore, a lens as shown in figure 5 was used to expand the beams to desired diameter.The beam splitter separated the expanded laser light beam into two branches. Mirrors were used to vary the direction of light beams. The dust particles that fall on optical instruments were cleaned regularly because they produce secondary reflections adversely affecting the quality of holograms.

Several techniques were used to improve upon flow visualization of the jet. Single and double exposure holograms were taken for comparison purposes. The transverse mode selector aperture was varied from 1.0 mm to 2.0 mm, with 0.5 mm increments; best lighting was obtained with the use of 1.5 mm aperture. For double exposure holograms the horizontal and vertical translations of the diffuser plate and hologram plate were used, varying from 0.001 inches to 0.005 inches. The vertical and horizontal translations yielded clear horizontal and vertical fringes, respectively. In the double exposure technique a static-dynamic exposure consisted of a no flow exposure, a diffuser or hologram plate translation, and finally an exposure with the jet flow.

Holograms were produced on Agfa-Gaevert 8E75 holographic plates, 4 inches by 5 inches in size. The development process included five minutes in Kodak D-19 developer, 30 seconds in a flowing water bath, five minutes

in standard fixer, one minute in a flowing water bath, fcllowed by immersion in Kodak Hypo-cleaning prior to drying..

2. Photographic technique

To reconstruct the image from the hologram, various methods can be employed. In the usual reconstruction method the hologram is re-illuminated by a beam similar to the original reference beam, as shown in figure 10 . Each individual point on the photograph is produced by many different non-parallel sets of rays originating from various source points on the diffuser plate in the beam that was used to construct the hologram. The spatial filtering technique which is shown in figure 11 allows a parallel set of rays selected by the positioning of a small aperture at the focal plane of the imaging lens. The resulting photographs are simpler to analyze since the angles are constant.

The technique employed in this work, which is easier to achieve than the previous two methods, is an application of the lensless focusing capability of the hologram. Figure 12 shows a hclogram which is re-illuminated by a conjugate reference beam of small diameter. The illuminated portion of the hologram covers a small aperture, since the reconstruction beam is of small size. The real image produced in this manner possesses large depth of field.

In this investigation recontruction was made by illuminating the hologram with a seven milliwatt continuous wave Helium-Neon laser as a conjugate reference beam at a wavelength of 6328 angstroms. There is slight distortion in the reccnstructed scene because of the difference in wavelength frcm the original scene beam. However, the effect is almost cancelled by shrinkage of holographic-plate

emulsion during the development process. The arrangment shown in figure 12 was used with the camera viewing screen in the position of the real image. The hologram was moved such that the best picture was obtained in the camera screen. A Polaroid type 55 Positive-Negative film was used with exposure times of from 0.2 to 0.5 seconds .

C. EXPERIMENTAL RESULTS AND DISCUSSION

In the case of a free jet, except at low Reynolds numbers, it is found that the jet becomes completely turbulent at a short distance from the orifice. The critical Reynolds number is startlingly low and is determined to be about 10 (Reference 8). In the present experiment holograms of the jet flow were taken at the nozzle exit velocities ranging from 200 ft/sec to 500 ft/sec with a corresponding Reynolds number range of 4×10^4 to 2.5×10^5. Hence the flow under the consideration was essentially turbulent.

Flow visualization of a steady turbulent jet was first studied by Bradshaw,et al.(Reference 9), and schlieren photographs of the turbulent jet were published in 1964. He determined that viscosity influences jet turbulence primarily by affecting the boundary layer shed from the nozzle and that the boundary layer depends on contraction upstream of the nozzle, as well as on the Reynolds number based on the exit speed and diameter. S.C.Crow, et al.(Reference 10) performed qualitative experiments with a water jet over a wide range of Reynolds numbers and reported orderly structure of the turbulent jet. Their results can be summarized with the help of figure 13. The first sign of instability was the sinuous, whiplash motion sketched in figure 13(a). The remaining parts of the figure show the effect of changing Reynolds number on the instability. As the Reynolds number advances, the sinuous column coils into

a corkscrew shape (b), then tightens and forms bulbous lobes like a crankshaft (c), and finally breaks into a train of axisymmetric puffs at the Reynolds number of the order of 10. The photographs of the holograms of a steady turbulent jet for this experiment are shown as figures 14, 15 and 16. figures 14 and 15 represent double exposed holograms and Figure 16 is a single exposure. The axisymmetric puff structure is clearly visible from the double exposed holograms, due to the contrast.The other kind of axisymmetric structure which is visible in the photographs is the pattern of surface ripples on the boundaries of the jet column. It is also observed from comparing these figures that the surface ripples shorten as Reynolds number increases. The crescent like shape of waves at the downstream of the jet is also observed in figure 16 and is due to the fact that the wave is retarded by the ambient air on both sides.

The holograms of the unsteady(oscillating) turbulent jet are shown as figures 17 through 23. These holograms clearly show that the jet is indeed flapping from side to side when the fluidic control ports of the nozzle are interconnected. This behavior of the jet was observed with schlieren methods as reported by Hermann Viets in Reference 6. The single exposure holograms of the oscillating jet shown as figures 17 and 18 show clearly the mixing between the jet flow and the entrained air. Distinct vortex puffs of jet air and pockets of entrainment air are visible in these photographs, thus showing a better mixing rate than for the steady jet. Figures 16 and 18 represent the holograms of the non-oscillating and oscillating jets respectively, at the same exit condition (same nozzle stagnation pressure). It is interesting to notice from these figures that the flapping jet retains the same symmetric structure as that of the steady jet. It was also observed in this investigation, and is evident from the oscillating jet holograms, that in all

cases the jet was at either of the two extreme flapping positions. Since the exposure time of the holograms was on the order of tens of nano-seconds, which is fast enough to freeze the flow, this behavior could be possible only if the time of the jet when it is attached to the walls is much greater (in order of magnitude) than the time it takes flapping from one side to the other. In other words this means that the jet remains attached to the wall for some interval of time until the bistable fluidic element raises the pressure there and rapidly pushes it to the other side. The sinusoidal pattern of waves in the oscillating jet as demonstrated by Hermann Viets ,et al. (Reference 11), was also not observed due to the short exposure time of the hologram. The crescent like wave structure at downstream of the jet,as observed for the case of the steady jet, is also visible in the holograms of the oscillating jet.

The spreading rate of the jet, defined as the half angle of the spread fan, was measured at different flow conditions and is plotted in figure 24. The half spread angle remained constant at about 10. This result shows that the assumption in Tollmien's theory that the spread rate of the turbulent jet increases linearly with the distance along the axis of the jet is a realistic one. Tollmien applied Prandtl's mixing length theory to solve the turbulent jet mixing problems (Reference 12). In the case of the unsteady (oscillating) turbulent jet the spread angle was measured to be about 20 degrees, about double the spreading rate of the non-oscillating jet. The spread rate is plotted in figure 25

III MEAN VELOCITY PROFILE INVESTIGATION

A. THEORY OF STEADY TWO-DIMENSIONAL TURBULENT FREE JETS

Qualitatively turbulent jet flow resembles that flow in laminar jets (Reference 13) but there are large quantitative differences which are due to much larger turbulent friction. Free turbulent flows are much simpler for mathematical analysis than flows along a wall, because turbulent friction is much larger than laminar friction in the whole region of a free turbulent jet . Hence, laminar friction may be wholly neglected in this analysis, which is not the case for the flow along the wall. It is also observed that the problems in free turbulent jet flow are of a boundary-layer nature, because the region in which a solution is desired does not extend far in a transverse direction as compared with the main direction of flow; and that the transverse gradients are larger. The boundary-layer equation for the two-dimensional case is

$$\frac{\partial u}{\partial t} + u\frac{\partial u}{\partial x} + v\frac{\partial u}{\partial y} = \nu\frac{\partial^2 u}{\partial y^2} \qquad (1)$$

where ν denotes the kinematic viscosity, and u and v represent components of velocity in the x and y directions as shown in figure 26. The pressure terms are dropped in the equation because in the free-jet flow it is permissible to assume that the pressure remains constant in the axisymmetric region.

In order to obtain the equation for steady mean flow in the turbulent jet it is convenient to separate the flow into a mean motion and into fluctuating or eddy motion. Denoting the time average of the u-component of velocity by $\overline{u}$ and its velocity of fluctuation by u', where the mean will be

taken over a sufficient long period of time t_1 , we write down the followng relations for the velocity components

$$u = \bar{u} + \acute{u} \quad , \quad v = \bar{v} + \acute{v} \qquad (2)$$

and

$$\bar{u} = \frac{1}{t_1} \int_{t_o}^{t_1} u \, dt$$

By substituting equation (2) into equation (1), and simplifying, the two-dimensional steady mean flow equation can be written as:

$$\bar{u} \frac{\partial \bar{u}}{\partial x} + \bar{v} \frac{\partial \bar{u}}{\partial y} = - \frac{\partial}{\partial y} (\overline{u'v'}) \qquad (3)$$

The momentum balance equation, obtained by integrating equation (3) over the boundary layer thickness δ , gives: (Reference 14)

$$\int_0^{\delta} \frac{\partial}{\partial x} (\bar{u}^2) \, dy = 0$$

Since $\bar{u}$ =0 on the edge of the jet, this result may be written as

$$\frac{d}{dx} \int_0^{\delta} \bar{u}^2 \, dy = 0$$

which implies,

$$\int_0^{\delta} \bar{u}^2 \, dy = \frac{1}{2} \frac{M_o}{\rho} = \text{Constant} \qquad (4)$$

where M_o is the (constant) momentum flux at the origin of the jet exit .

Now from Prandtls hypothesis and experimental results it is known that for free flows, such as jets or wakes, the exchange ccefficient or virtual kinematic viscosity, defined by

$$\epsilon = - \frac{\overline{u'v'}}{\partial \bar{u}/\partial y} \qquad (5)$$

is almost independent of y . According to Prandtl's hypothesis ,

$$\epsilon \propto (U_{max} - U_{min})\,\delta \qquad (6)$$

where U_{max} and U_{min} are the maximum and minimum velocities in the cross-section (Reference 13,14). In the case of two-dimensional turbulent free jets

$$U_{min} = 0 \quad , \quad U_{max} \propto x^{1/2} \quad , \quad \delta \propto x \qquad (7)$$

so ϵ is a function of x only (Reference 13). Thus equation (5) implies that

$$-\overline{u'v'} = \epsilon(x)\,\frac{\partial \bar{u}}{\partial y}$$

Substituting equation (8) into equation (3), the equation of

mean flow becomes

$$\bar{u}\,\frac{\partial \bar{u}}{\partial x} + \bar{v}\,\frac{\partial \bar{u}}{\partial y} = \epsilon(x)\,\frac{\partial^2 u}{\partial y^2} \qquad (9)$$

Let us recall the stream function ψ , which is defined by

$$\bar{u} = \frac{\partial \psi}{\partial y} \quad , \quad \bar{v} = \frac{\partial \psi}{\partial x}$$

and substitute it into equation (9), obtaining the equation of motion, in terms of mean stream function ψ , as

$$\frac{\partial \psi}{\partial y}\,\frac{\partial^2 \psi}{\partial x \partial y} - \frac{\partial \psi}{\partial x}\,\frac{\partial^2 \psi}{\partial y^2} = \epsilon(x)\,\frac{\partial^3 \psi}{\partial y^3} \qquad (10)$$

Now let us change the independent variable x to X , where

$$X = \int_0^x \epsilon(x)\,dx \,. \qquad (11)$$

Then equation (10) becomes

$$\frac{\partial \psi}{\partial y}\,\frac{\partial^2 \psi}{\partial X \partial y} - \frac{\partial \psi}{\partial X}\,\frac{\partial^2 \psi}{\partial y^2} = \frac{\partial^3 \psi}{\partial y^3} \qquad (12)$$

Equation (12) has the same form as the laminar jet equation with ν =1. The solution of equation (12) is therefore,

(Reference 14),

$$\psi = 2\,C\,X \tanh\left(\frac{Cy}{3X^{2/3}}\right) \qquad (13a)$$

and

$$\bar{u} = \frac{2}{3}\,\frac{C^2}{X^{1/3}}\,\mathrm{Sech}^2\,\xi \qquad (13b)$$

where

$$\xi = \frac{Cy}{3X^{1/3}} \quad \text{and} \quad C = \left(\frac{9M_o}{16\rho}\right)^{1/3}$$

The constant M_o, the momentum flux, can be calculated at the origin.

In order to obtain the mean velocity in terms of actual co-ordinates (x,y) we use the results of equations (6) and (7) and obtain

$$\epsilon = \epsilon_o\, x^{1/2} \qquad \text{where} \qquad \epsilon_o = \text{Constant}$$

Substituting the above result into equation (11) one obtains

$$X = \epsilon_o\, x^{3/2} \qquad (14)$$

Substituting equation (14) into (13), the velocity profile

may be written as

$$\bar{u} = C^{3/2}\left(\frac{46}{3x}\right)^{1/2} \operatorname{Sech}^2\left(\frac{6y}{x}\right) \qquad (15)$$

where

$$6 = \frac{C}{3(2/3\epsilon_0)^{2/3}}$$

is a dimensionless constant which is determined experimentally to be about 10.

B. EXPERIMENTAL APPARATUS

1. Laser Doppler Anemometer

The DISA 55L Laser Doppler Anemometer Mark II was used to measure the mean velocities in this experiment. A Doppler anemometer measures the velocity of a target, generally a moving fluid, by observing the frequency shift in the scattered light due to the velocity of the target. The Doppler frequency is measured by mixing the shifted signal beam with the original reference beam and observing the beats between them. This measuring technique therefore requires that the flow medium be translucent and contain particles which scatter light as shown in figure 27(a). Figure 27(b) shows the geometry of this principle. The unit vectors $\hat{e}_i$ and $\hat{e}_s$ are defined in the direction of the incident and scattered light waves, respectively, and $\bar{V}$ represents the velocity of the particle.

The frequency relationship between a scattered light wave and the light wave from which it originates is given by the equation (Reference 15):

$$f_s = f_i + \frac{1}{\lambda} \overline{V} \cdot (\hat{e}_s - \hat{e}_i) \qquad (1)$$

where

f_s = Frequency of scattered light

f_i = Frequency of incident light

λ = Wave length of incident light

$\overline{V}$ = Velocity vector of particle

$\hat{e}_s$ = Unit vector in scattering direction

$\hat{e}_i$ = Unit vector in incident direction

The frequency shift is equal to the Doppler frequency, f_D

$$f_D = f_s - f_i \qquad (2)$$

From equation (1) and (2), one determines

$$f_D = \frac{1}{\lambda} \overline{V} \cdot (\hat{e}_s - \hat{e}_i) \qquad (3)$$

The above equation indicates that the Doppler frequency is directly proportional to the particle velocity.

Figure 28 shows a typical arrangement of optics in laser anemometry. The anemometer uses two incident beams where the beam intersection forms the point of measurement in the flow. The scattered light is collected by the photomultiplier. Equation (3) can be rewritten for two intersecting beams as :

$$f_D = \frac{1}{\lambda} V \, 2 \, \text{Sin} \frac{\theta}{2}$$

or

$$V = \frac{f_D \lambda}{2 \, \text{Sin} \frac{\theta}{2}} \qquad (4)$$

where V is the component of local flow velocity and θ is the angle of beam intersection. The above equation can be simplified into:

$$V = C \, f_D$$

where

C = Calibration factor in M/Sec/MHz and is given by

$$C = \frac{\lambda}{2 \, \text{Sin} \frac{\theta}{2}}$$

Major features of the Mark II Anemometer are contactless velocity probing and digital velocity display directly in meters/sec, independently of fluid temperature,

pressure and density when the correct setting of the calibration factor is used.

C. EXPERIMENTAL PROCEDURE

A line diagram of the arrangement used for the jet velocity measurements is shown in figure 29 and the photographs of the experimental setup are included as figures 30 and 31. The optical anemometer components shown in figure 29, except the data processing equipment, were mounted on a rigid platform, isolated from the nozzle to avoid nozzle vibration interference. The laser and integrated optical unit were mounted on an optical bench for better alignment. The nozzle was attached to an accurate vertical traversing mechanism driven by an electric motor to facilitate velocity survey across the jet.

The air in the jet flow was seeded with the smoke produced by heating kerosene oil in a smoke generator. The smoke generator, shown in figure 32 , was pressurized and contained six separately controlled bottles to cater to the varying seeding requirements, because the particle concentration decreased with axial and transverse distance due to entrainment. A 15 mW Helium-Neon laser provided the high intensity collimated light beam, which was split into two beams of equal intensity by the integrated optical unit described in Reference 5. The angle between the beams was varied and a value of 15.8 degrees was used with a 30 cm lens for this experiment. The light collecting system consisted of a single 30 cm lens and a variable field stop device mounted on an extension to the photomultiplier housing.

D. EXPERIMENTAL RESULTS AND DISCUSSION.

A comprehensive experimental and theoretical investigation of the bulk properties of turbulent, incompressible air jets issuing into stationary ambient air was presented by Sforza et al., in Reference 16. The flow fields of such jets were found to be characterized by three distinct regions of the axis velocity decay (figure 33). These regions may be classified as follows:

1. Potential core(PC) region: In this region the mixing initiated at the jet boundaries has not yet penetrated the entire flow field, thus leaving a region that is characterized by a constant axis velocity close to the jet exit velocity.

2. Characteristic decay(CD) region: In this region axis velocity decay is dependent upon the orifice configuration of the jet nozzle, and the velocity profiles are non-axisymmetric.

3. Axisymmetric type decay(AD) region: The axis velocity decay in this region is axisymmetric in nature independent of the orifice geometry. The velocity profiles in this region are found to be similar to those predicted by theory (Equation 15).

The above regions for the single element nozzle used in this investigation were calculated from the results of Reference 16 and are labelled in Figure 33. In order to verify the existence of these regions, a centerline velocity survey was made and is presented in figure 34.

The centerline velocity survey indicates much shorter

potential core and characteristic decay regions than the results obtained from Reference 16. This disagreement is due to the fact that the nozzle (Figure 3) under investigation had a fluidic element at the exit which enhanced the mixing in the downstream region.

The mean velocity profile surveys of the steady turbulent jet in the axisymmetric region were made at downstream axial distances of 15 cm and 40 cm. These profiles are shown in figures 35 and 36. Figure 37 is a result of a pitot tube survey at 15 cm. A nondimensionalized plot (figure 38) of the mean velocity profiles of figures 35, 36, and 37 was made to show the axisymmetric characteristic of the mean velocity decay and also to compare the experimental results with the theory and other published results (Reference 12). Velocity measurements near the jet boundary were not possible with the laser Doppler anemometer due to the mixing of entrained air with the jet flow, which decreased the smoke particles concentration and caused poor validation rates.

Mean velocity profile surveys of the unsteady (oscillating) jet were also made at the downstream distances of 15 and 40 cm from the exit and are presented in figures 39 and 40, respectively. The survey results demonstrate double peak velocity profiles, as reported in Reference 6. This type of profile can be explained and is due to the fact, previously illustrated by the holograms, that in the case of unsteady (oscillating) flow the jet remains attached to either side of the wall for some time and then quickly (comparatively shorter interval of time) flaps to the opposite side. The velocity profile peaks get farther apart as the distance from the jet exit increases (figures 39 and 40) and is due to the spreading of the jet as discussed in the earlier portion of this thesis. The difference in the peak velocity magnitudes, as seen in figures 39 and 40, is

caused by the fact that the jet tends to stay at one side for a longer duration than on the other side. This could be caused by the design of the fluidic element of the nozzle which controls the flapping phenomenon. For the same nozzle exit condition and downstream distance, the mean velocities of the unsteady jet are observed to be smaller in magnitude than that of the steady jet due to the enhanced mixing rates of the unsteady jet. Comparison of the mean velocity profile of the oscillating jet with other published results was not made because in the case of the oscillating jet the spreading and mixing rates are strongly dependent on the type of the fluidic element used (Reference 6).

IV. CONCLUSIONS

The holcgraphic technique for the flow visualization has been applied successfully to the study of structure, spreading rates of the steady and unsteady turbulent jet and the flapping phenomenon of the oscillating jet. The Dye-Switch Laser used in this investigation has a light pulse duratien of about 20 nano-seconds which is fast enough to freeze the flow field during the hologram construction process. The holograms of the turbulent air jet obtained during this investigation were of better quality than the photographs obtained by the other flow visualisation techniques. The mean velocity profile measurements obtained by the laser Doppler anemometer compared well with the theory and published results. The seeding requirements for the laser Doppler anemometer proved to be the most critical since the particle concentration decreased with the axial and transverse distance. In order to obtain velocities at the edge of the jet, seeding of the entrained air should be tried in further investigation on jet velocity profile. It may be concluded from present velocity survey results that the laser Doppler anemometer can be conveniently used in jet flows and can attain precision of measurements at least as good as available alternatives.

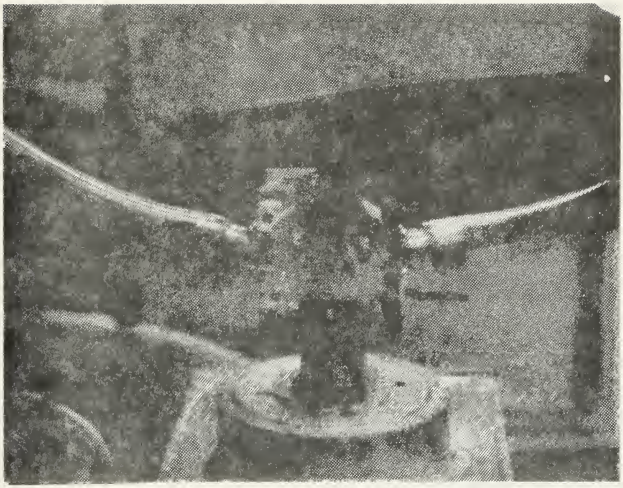

FIGURE 1. THE SINGLE ELEMENT NOZZLE

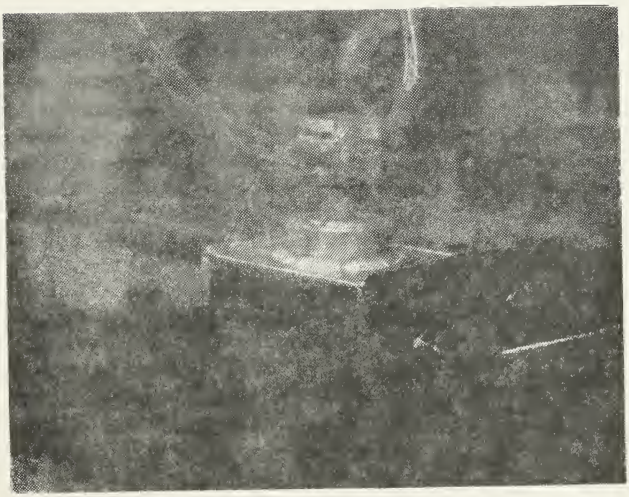

FIGURE 2. THE JET NOZZLE ASSEMBLY

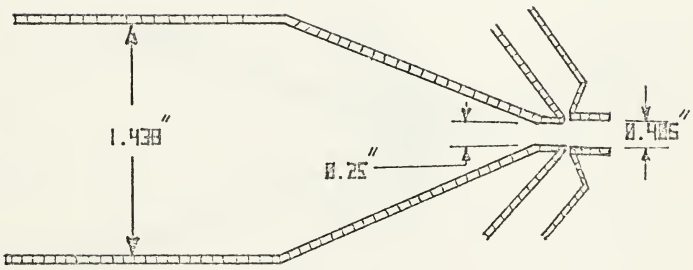

FIGURE 3. SINGLE ELEMENT NOZZLE

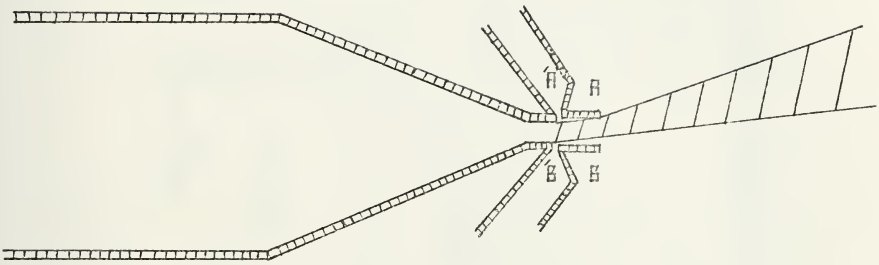

FIGURE 4. SCHEMATIC OF SIMPLE FLUIDIC ELEMENT

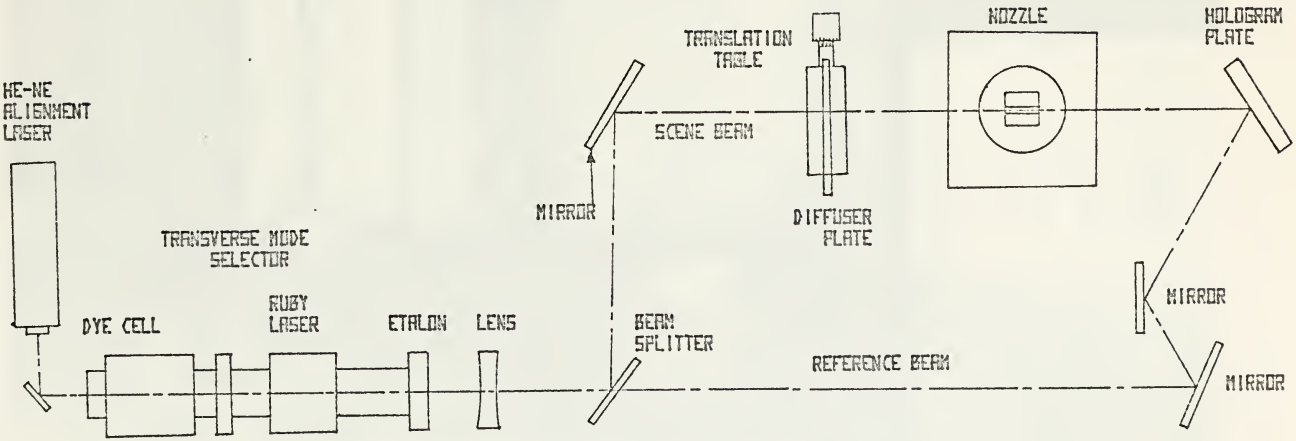

FIGURE 5. SCHEMATIC DRAWING OF THE HOLOGRAPHIC ARRANGEMENT

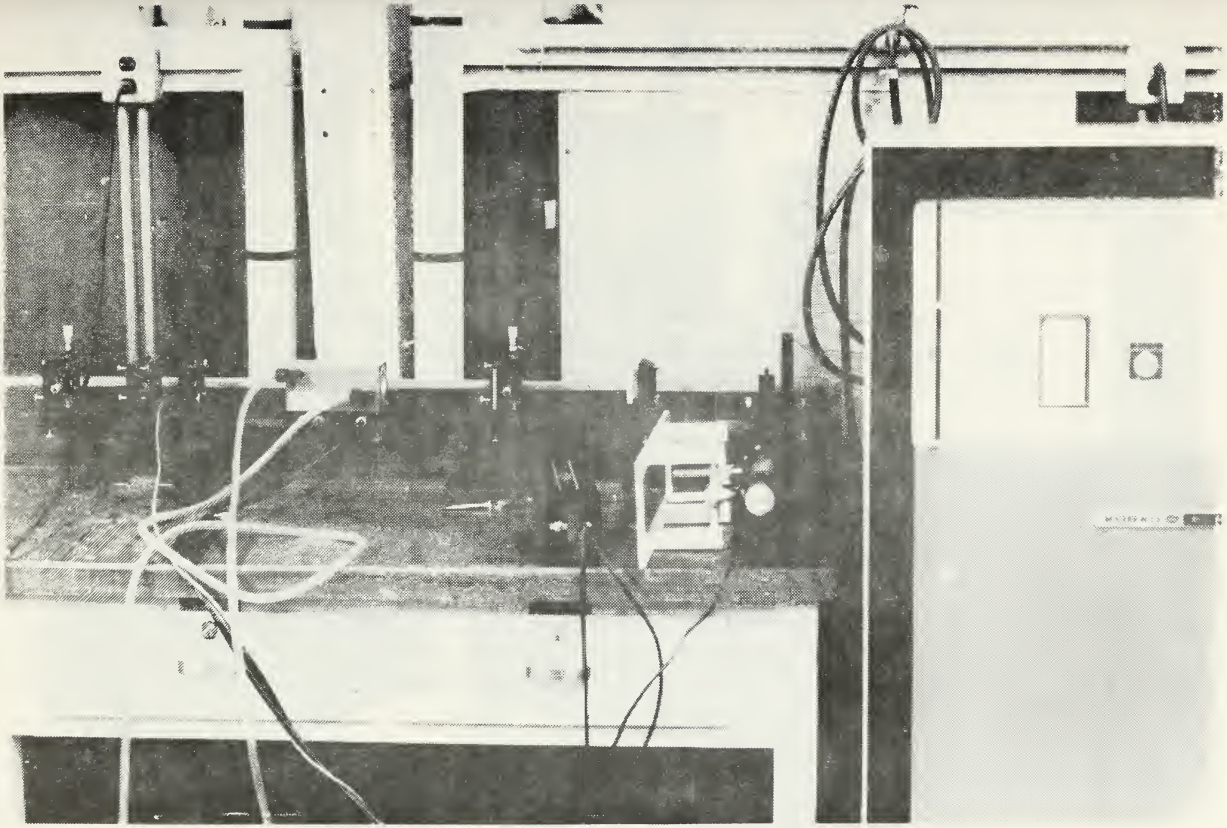

FIGURE 5. VIEW OF THE DYE-SWITCH UNIT ON THE DISTRIBUTION TABLE.

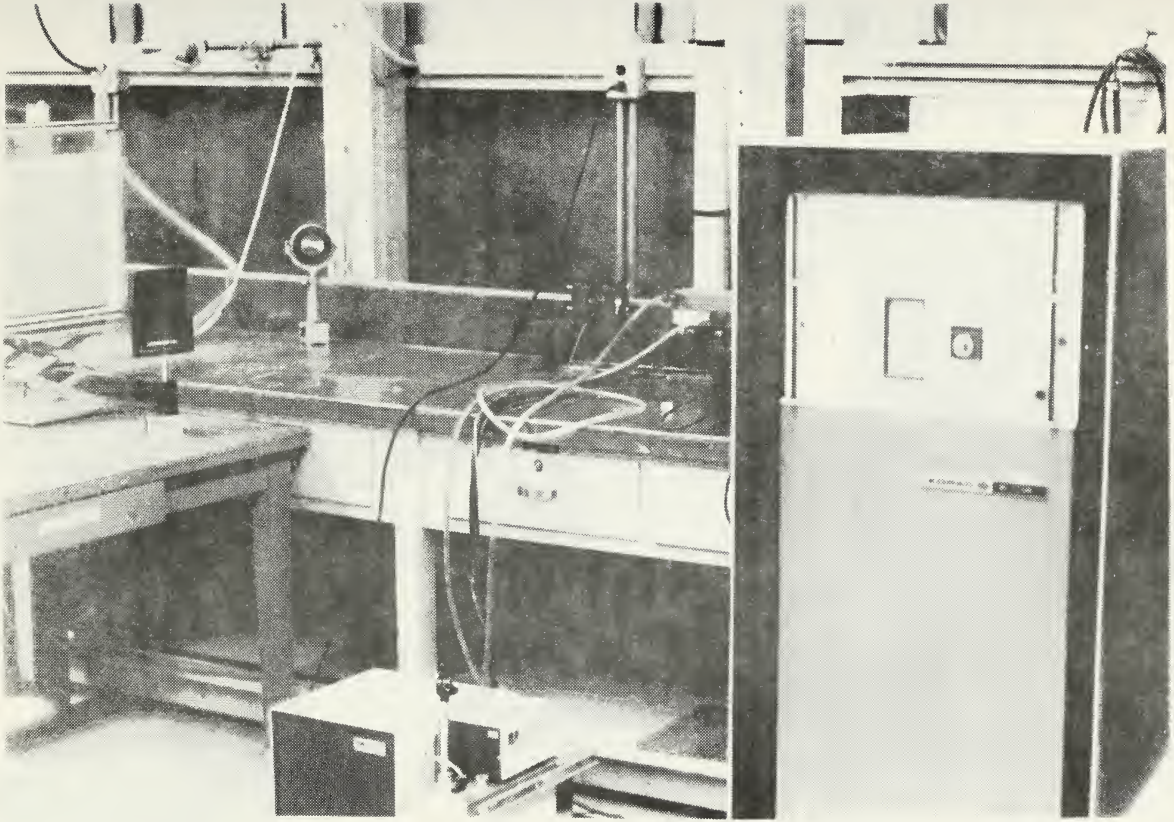

FIGURE 7. FIRING AND CONTROL UNITS OF THE OXY-GAS TORCH.

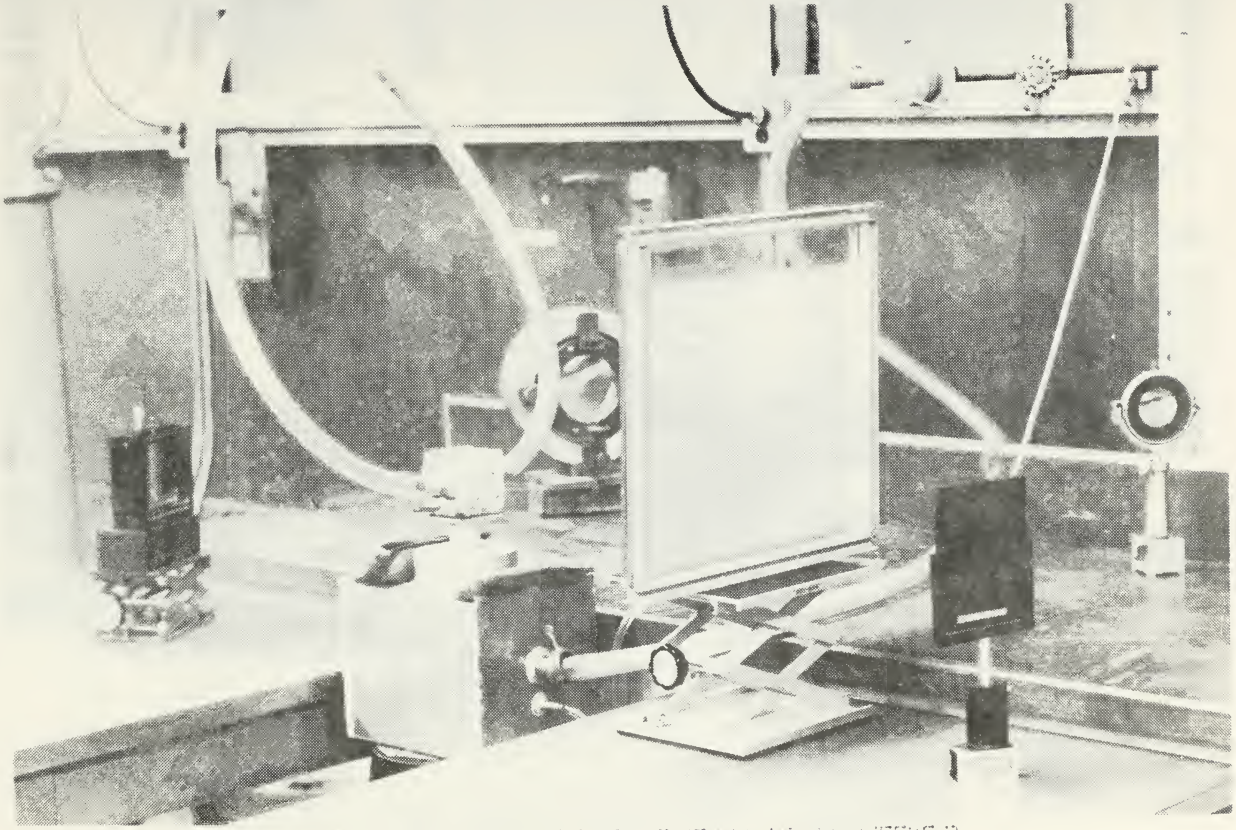

FIGURE 6. FRONT VIEW OF THE [illegible]

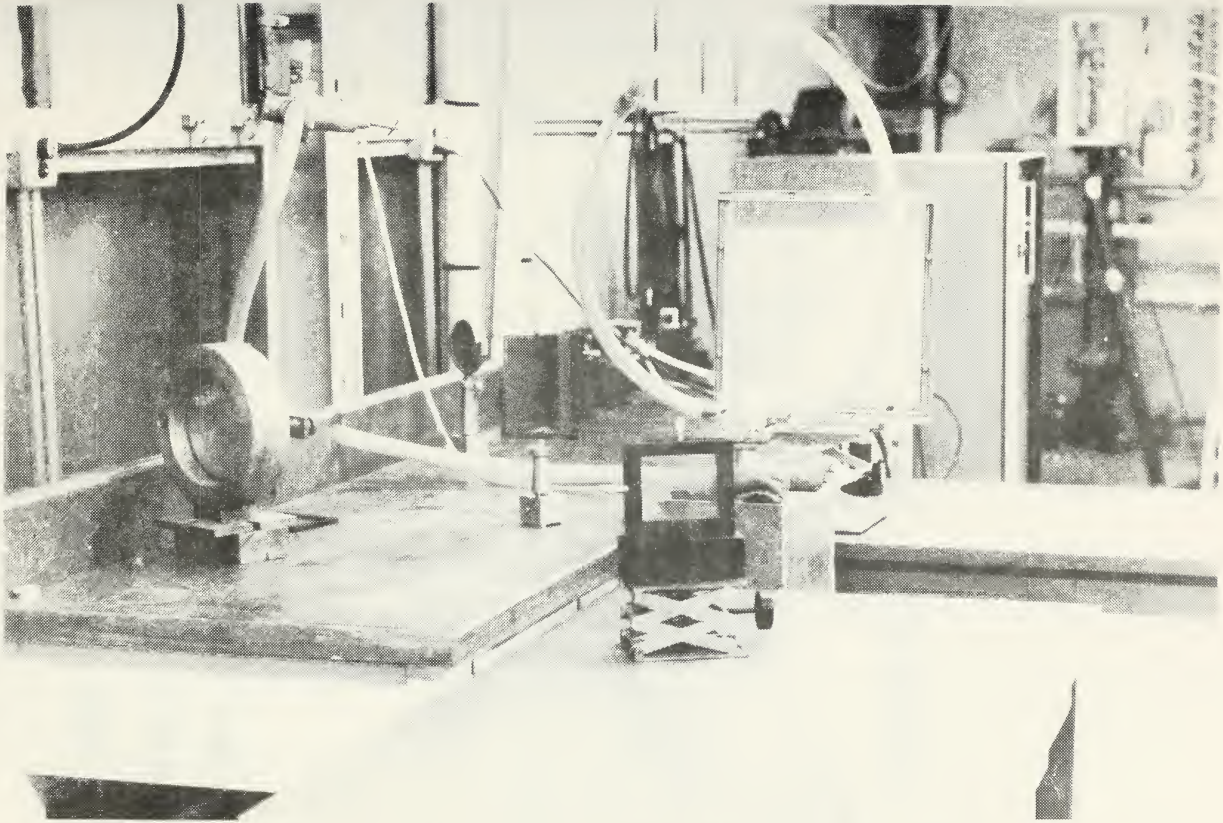

FIGURE 5. REAR VIEW OF THE MAGNETIC ARRANGEMENT

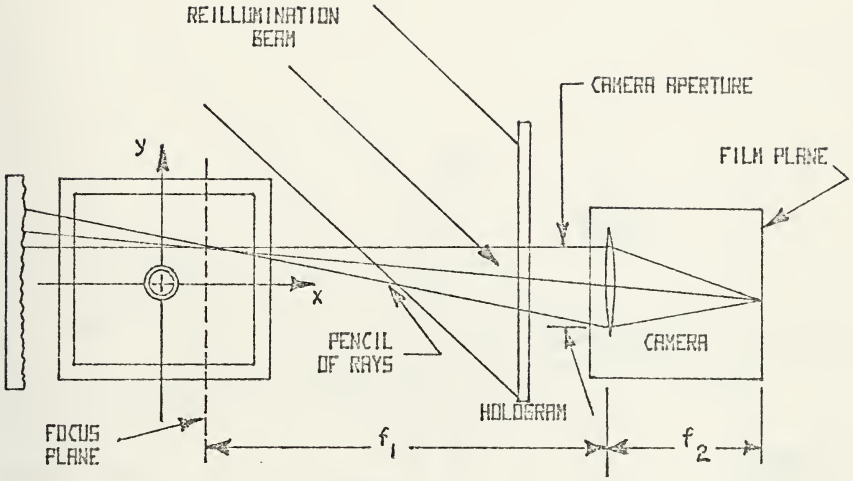

FIGURE 10. EFFECT OF APERTURE SIZE FOCUS PLANE POSITION ON THE PENCIL SIZE OF RAYS ABOUT A LINE OF SIGHT RECORDED BY CAMERA

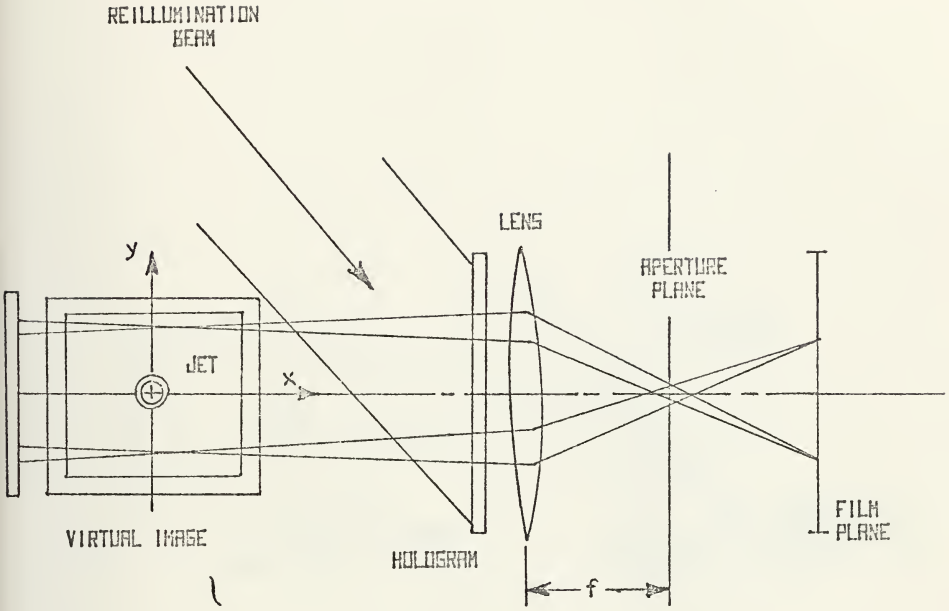

FIGURE 11. SPATIAL FILTERING TECHNIQUE FOR SELECTING PHOTOGRAPH OF CONSTANT ANGLE LINES OF LIGHT

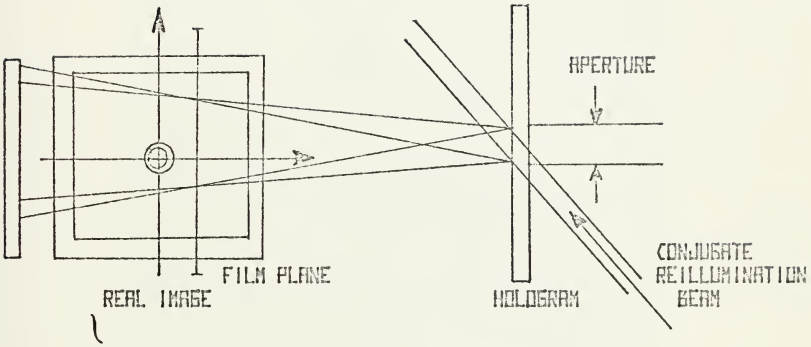

FIGURE 12. LENSLESS PHOTOGRAPHIC TECHNIQUE USING A CONJUGATE REFERENCE BEAM OF SMALL DIAMETER

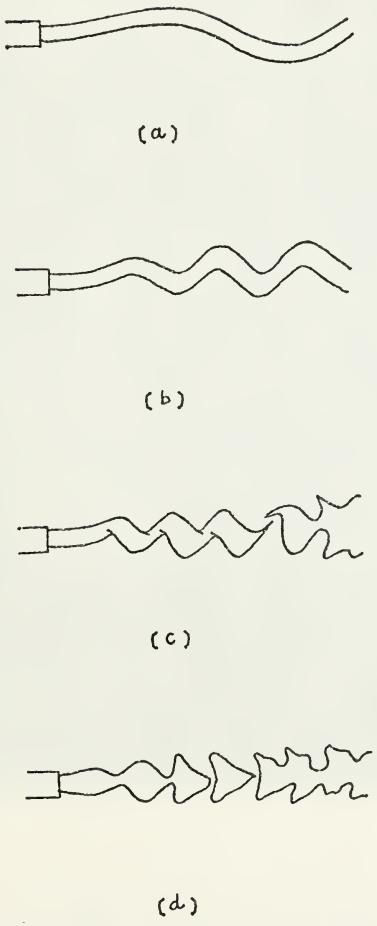

FIGURE 13. JET INSTABILITY WITH ADVANCING REYNOLDS NUMBER (10^2 - 10^3)

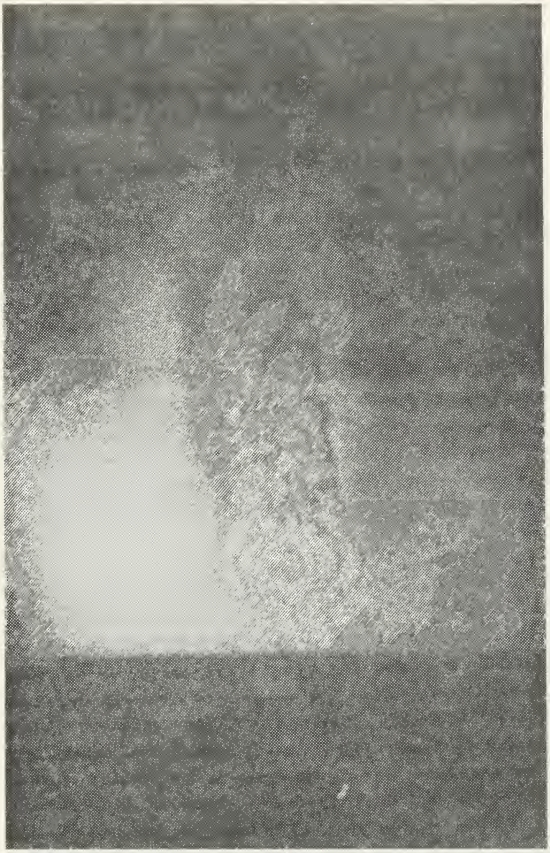

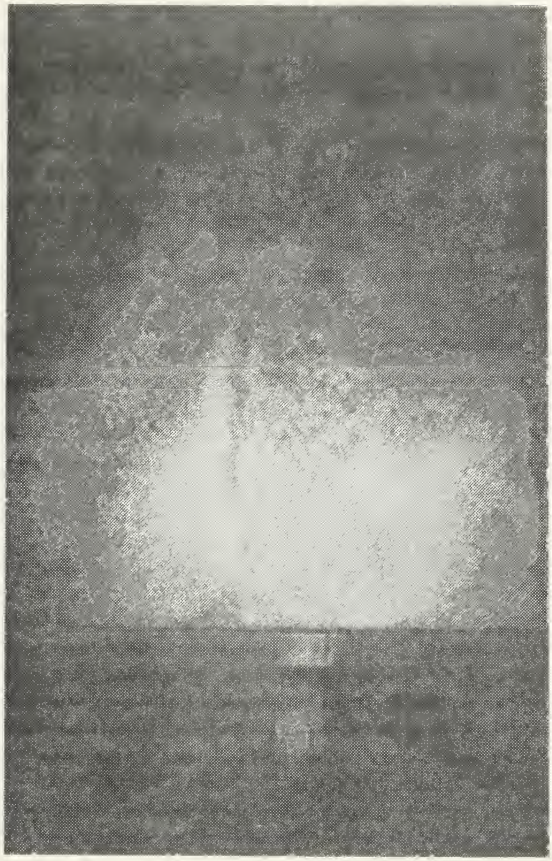

FIGURE 15. DOUBLE EXPOSURE HOLOGRAM OF STEADY JET
(REYNOLDS NUMBER 1.55×10^5)

FIGURE 16. SINGLE EXPOSURE HOLOGRAM OF STEADY JET
(REYNOLDS NUMBER 1.32×10^5)

FIGURE 17. SINGLE EXPOSURE HOLOGRAM OF UNSTEADY JET
(REYNOLDS NUMBER 1.25×10^5)

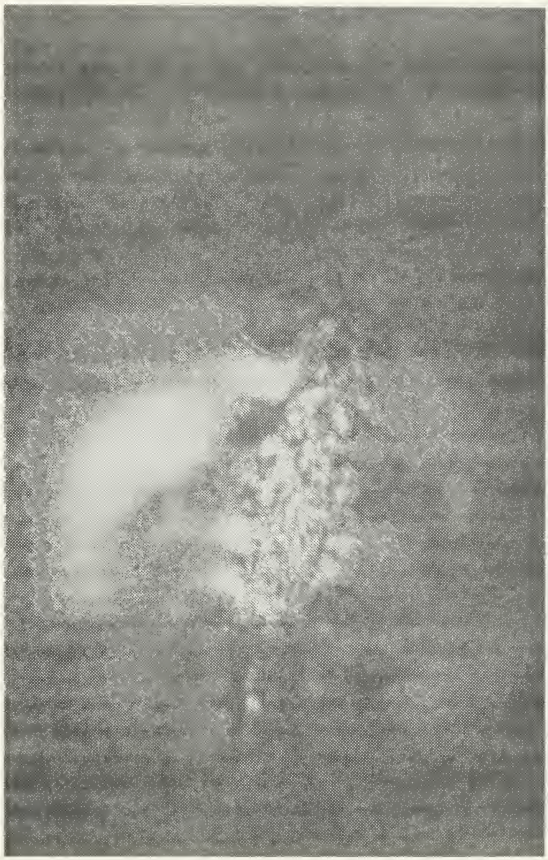

FIGURE 18. SINGLE EXPOSURE HOLOGRAM OF UNSTEADY JET (REYNOLDS NUMBER 1.32×10^5)

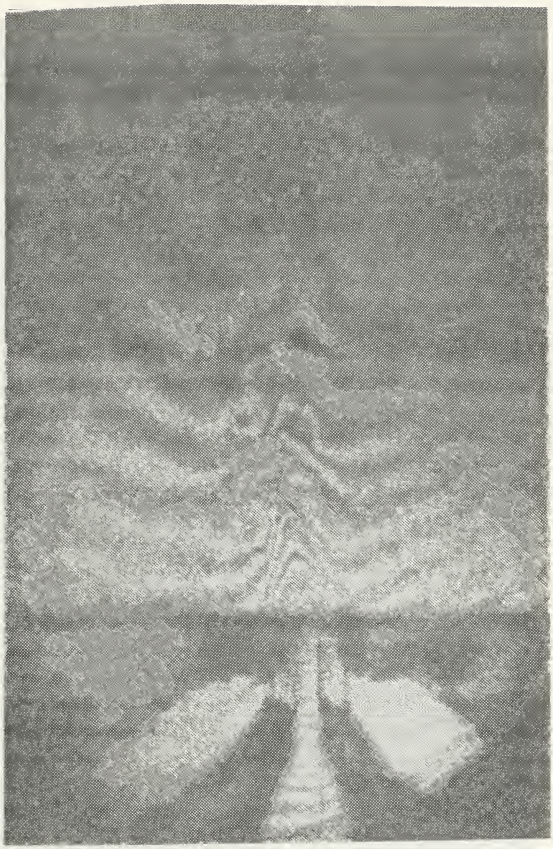

FIGURE 19. DOUBLE EXPOSURE HOLOGRAM OF UNSTEADY JET
(REYNOLDS NUMBER 1.38×10^5)

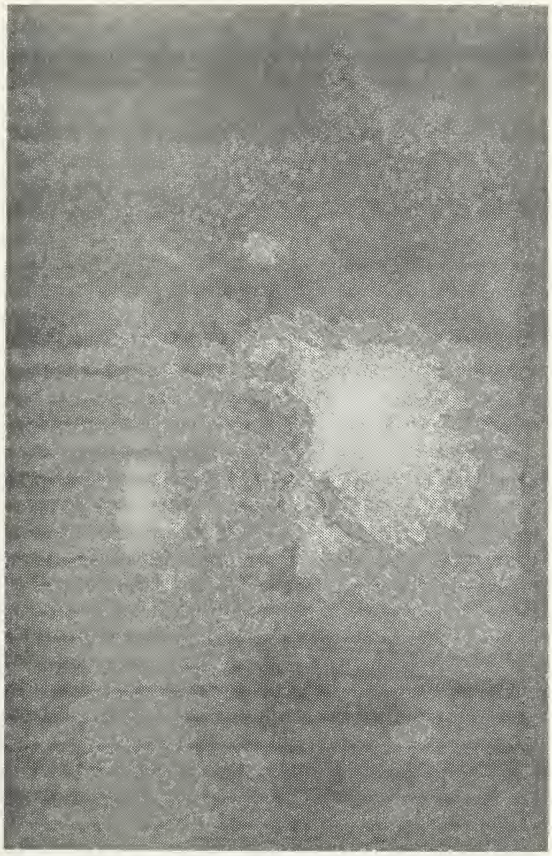

FIGURE 20. SINGLE EXPOSURE HOLOGRAM OF UNSTEADY JET (REYNOLDS NUMBER 1.45×10^5)

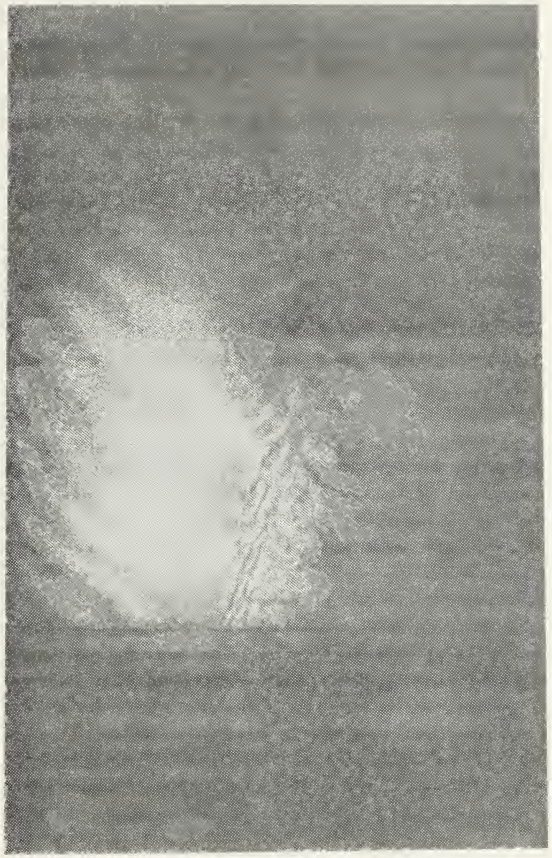

FIGURE 21. DOUBLE EXPOSURE HOLOGRAM OF UNSTEADY JET
(REYNOLDS NUMBER 1.55×10^5)

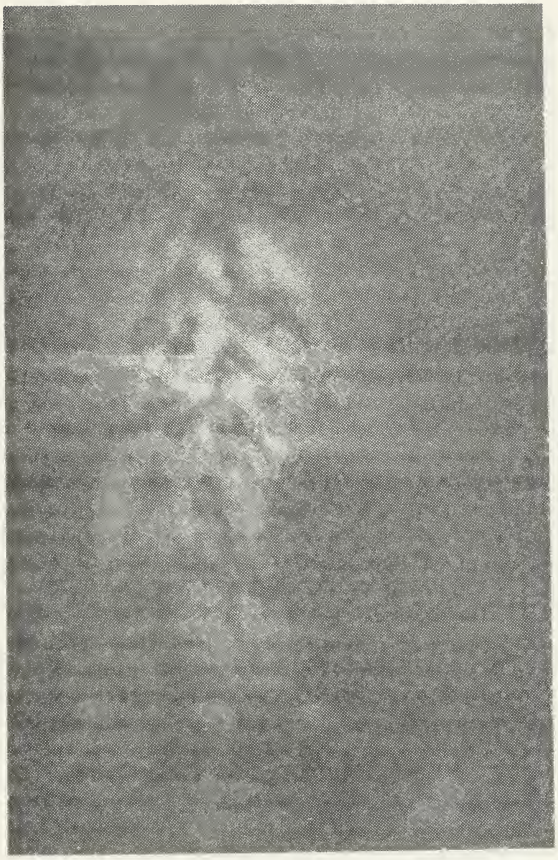

FIGURE 22. SINGLE EXPOSURE HOLOGRAM OF UNSTEADY JET
(REYNOLDS NUMBER 9×10^4)

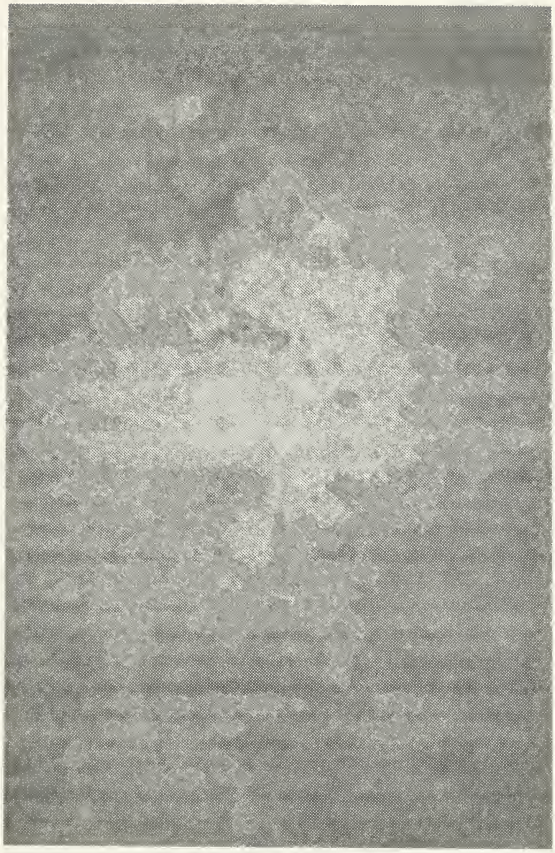

FIGURE 23. SINGLE EXPOSURE HOLOGRAM OF UNSTEADY JET
(REYNOLDS NUMBER 1.88×10^5)

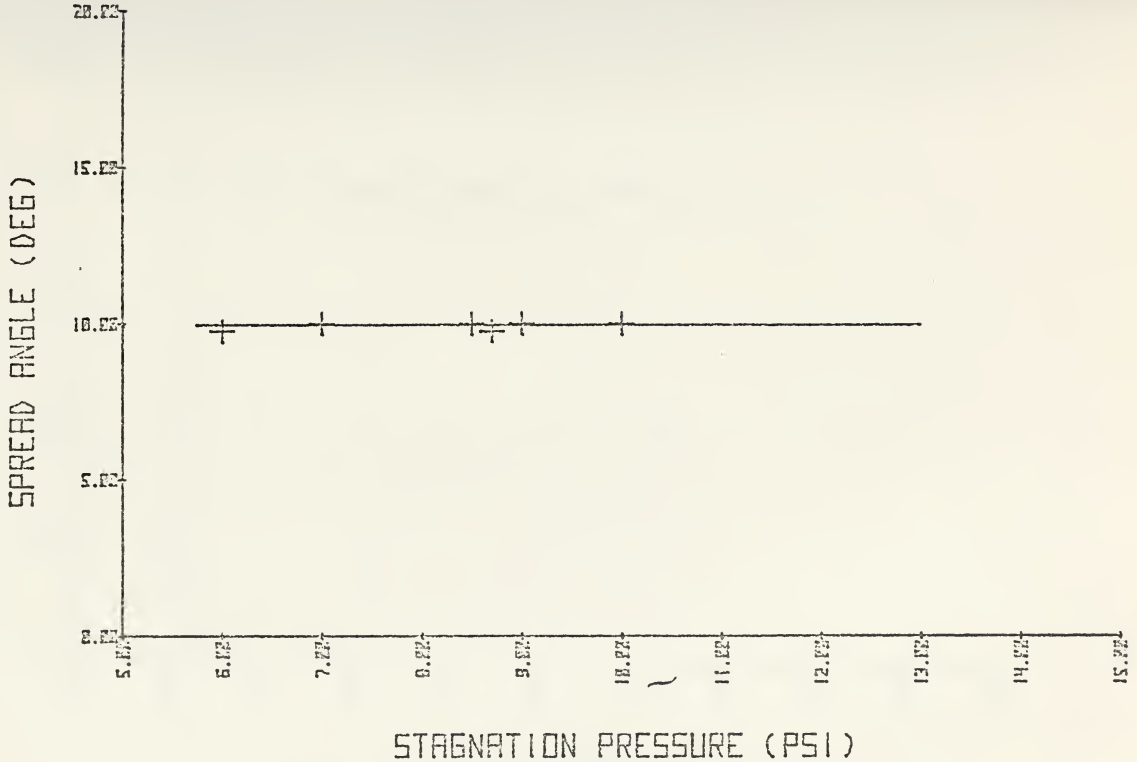

FIGURE 24. SPREADING RATE OF STEADY (NONOSCILLATING) JET (REYNOLLDS NUMBER RANGE $5X10^4$-$2X10^5$)

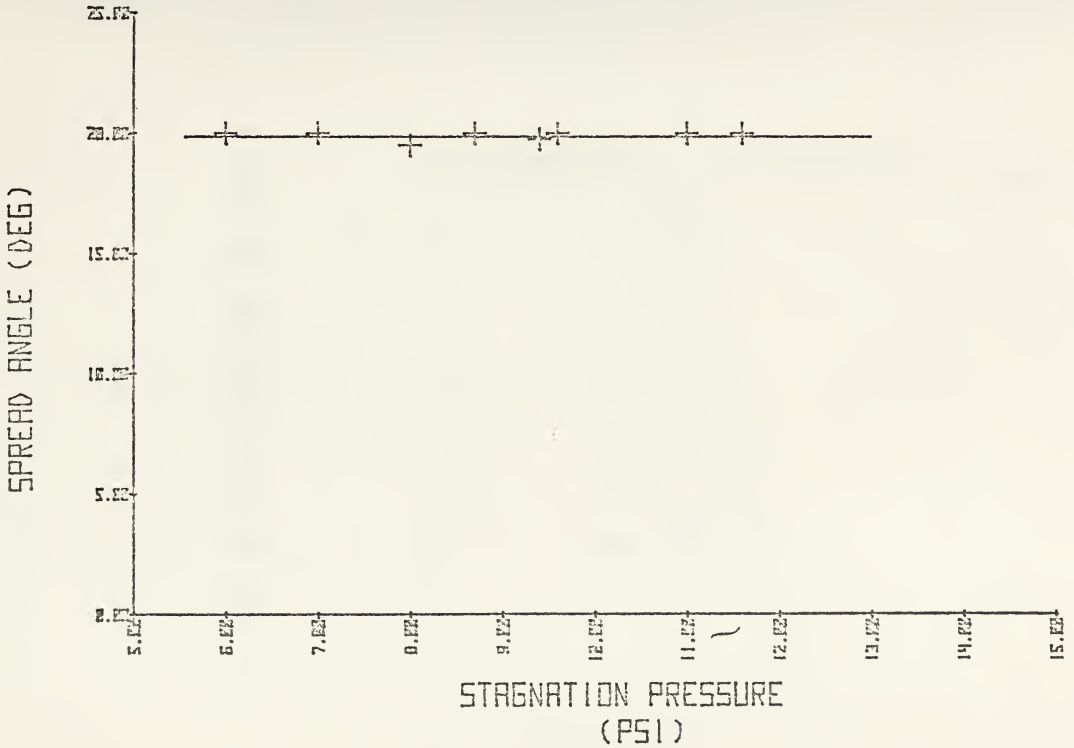

FIGURE 25. SPREADING RATE OF UNSTEADY (OSCILLATING) JET
(REYNOLDS NUMBER RANGE $5X10^4$-$2X10^5$)

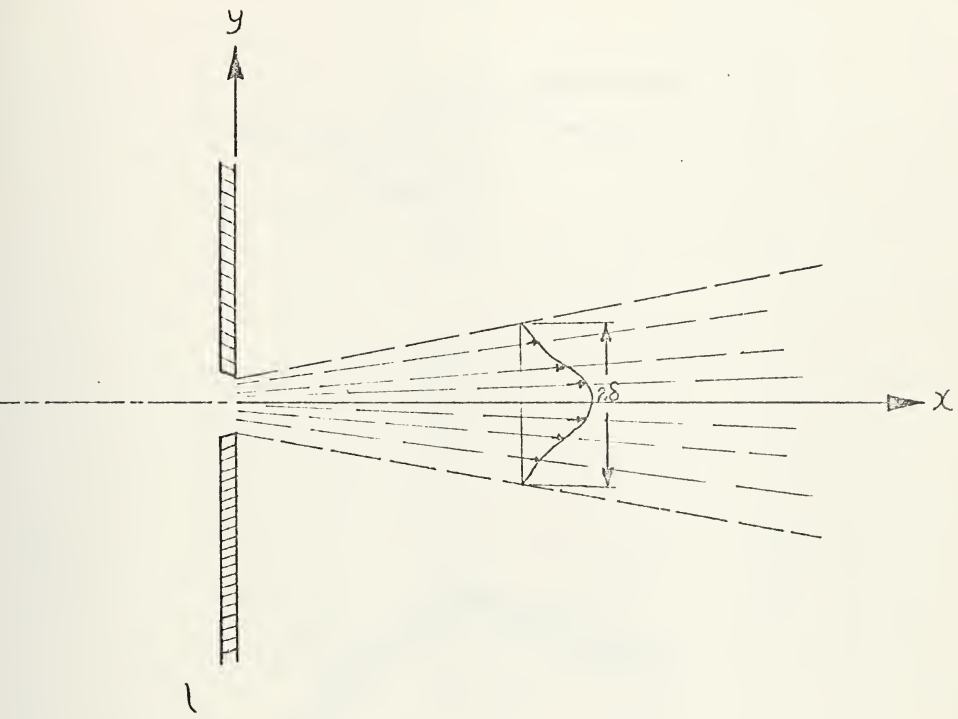

FIGURE 26. REFERENCE AXIS OF THE JET

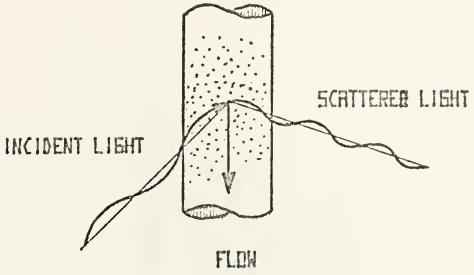

(a)

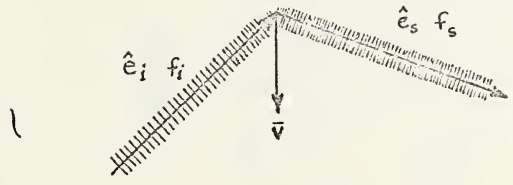

(b)

FIGURE 27. (a) PRINCIPLE OF LASER ANEMOMETRY
(b) GEOMETRIC REPRESENTATION OF (a)

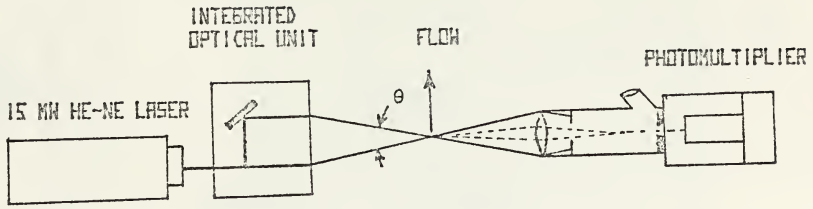

FIGURE 28. TYPICAL ARRANGEMENT OF OPTICS IN LASER ANEMOMETRY

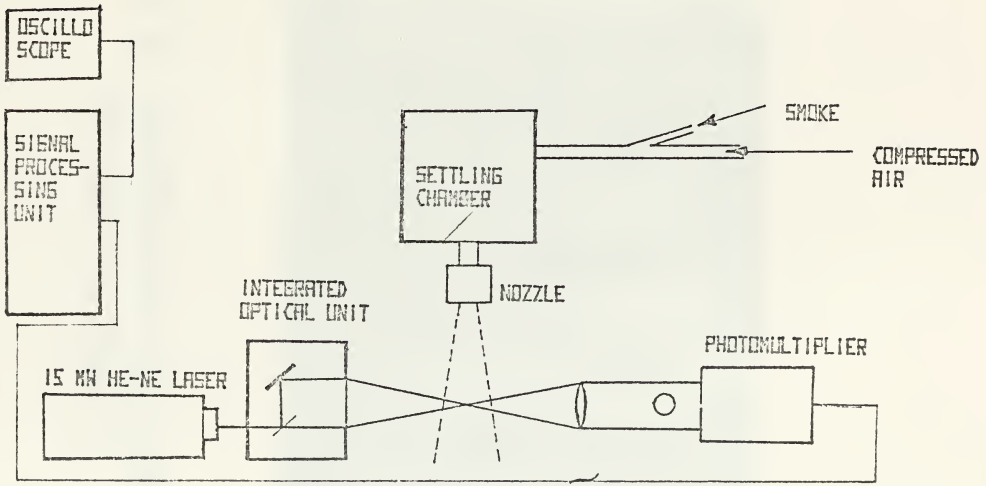

FIGURE 29. LINE DIAGRAM OF EXPERIMENTAL ARRANGEMENT FOR MEAN VELOCITY MEASUREMENTS

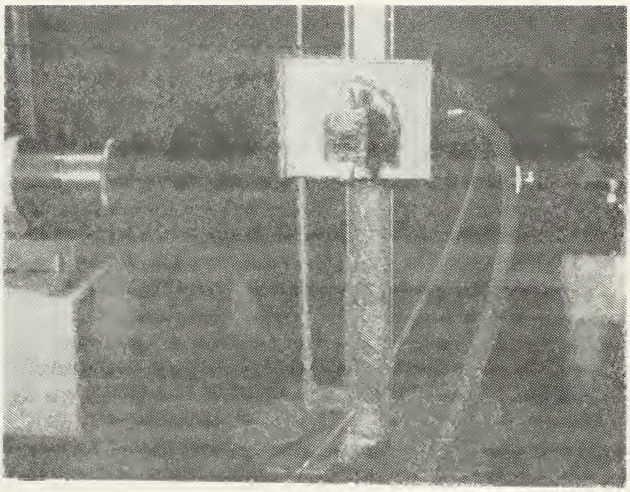

FIGURE 30. EXPERIMENTAL SET UP OF LASER ANEMOMETER AND TRAVERSING MECHANISM

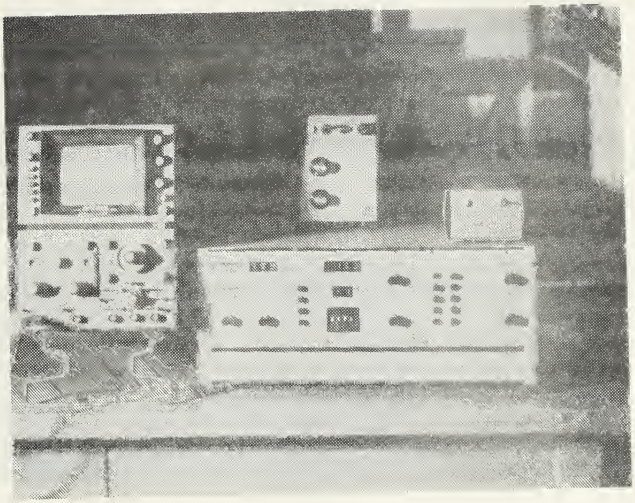

FIGURE 31. SSL90 LDA COUNTER PROCESSOR WITH OSCILLOSCOPE MONITOR

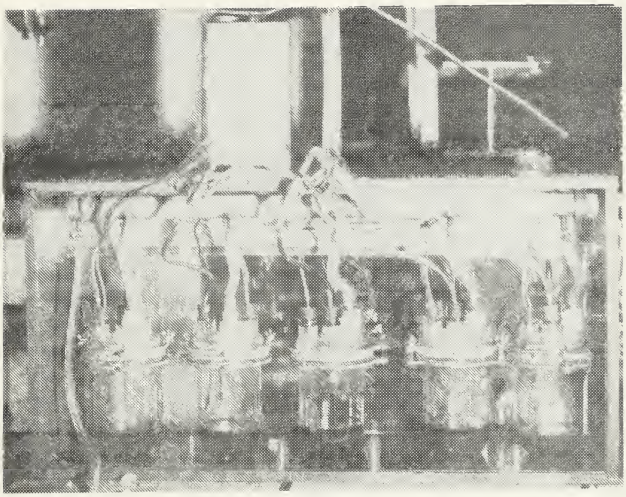

FIGURE 32. THE SMOKE GENERATOR FOR SEEDING REQUIREMENT

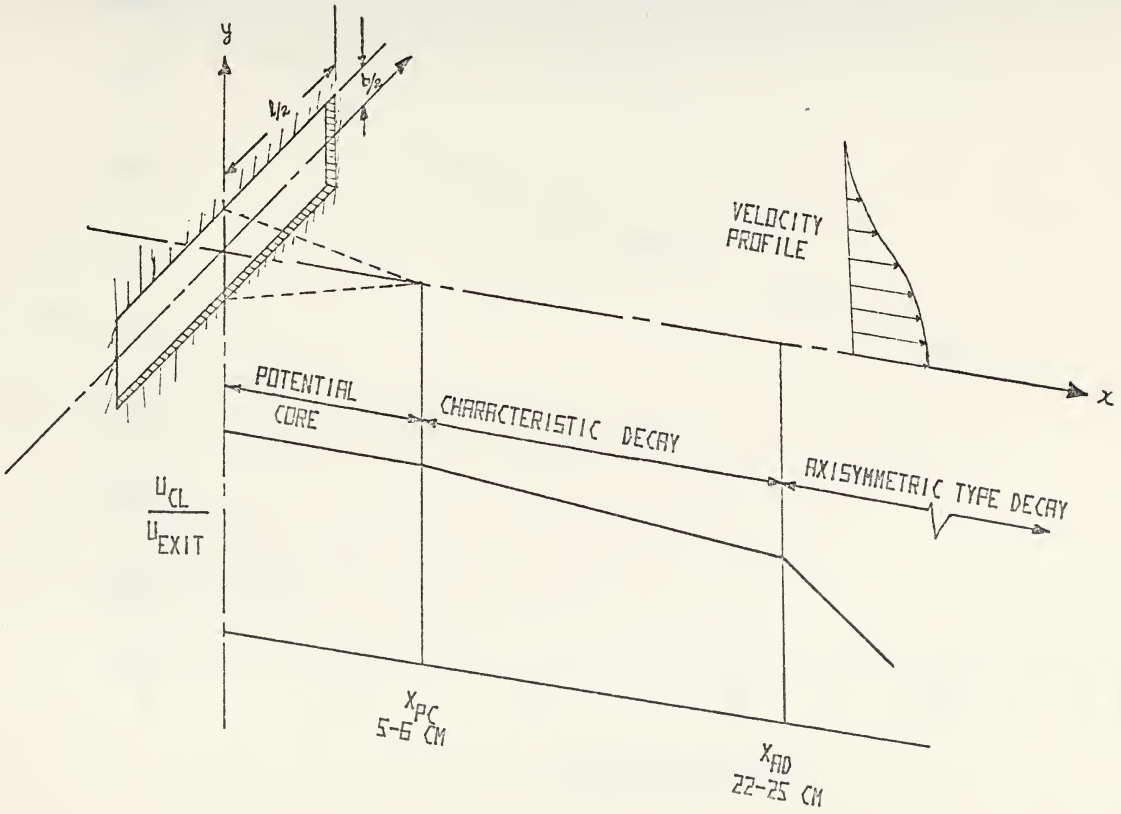

FIGURE 33. CENTER LINE VELOCITY DECAY REGIONS

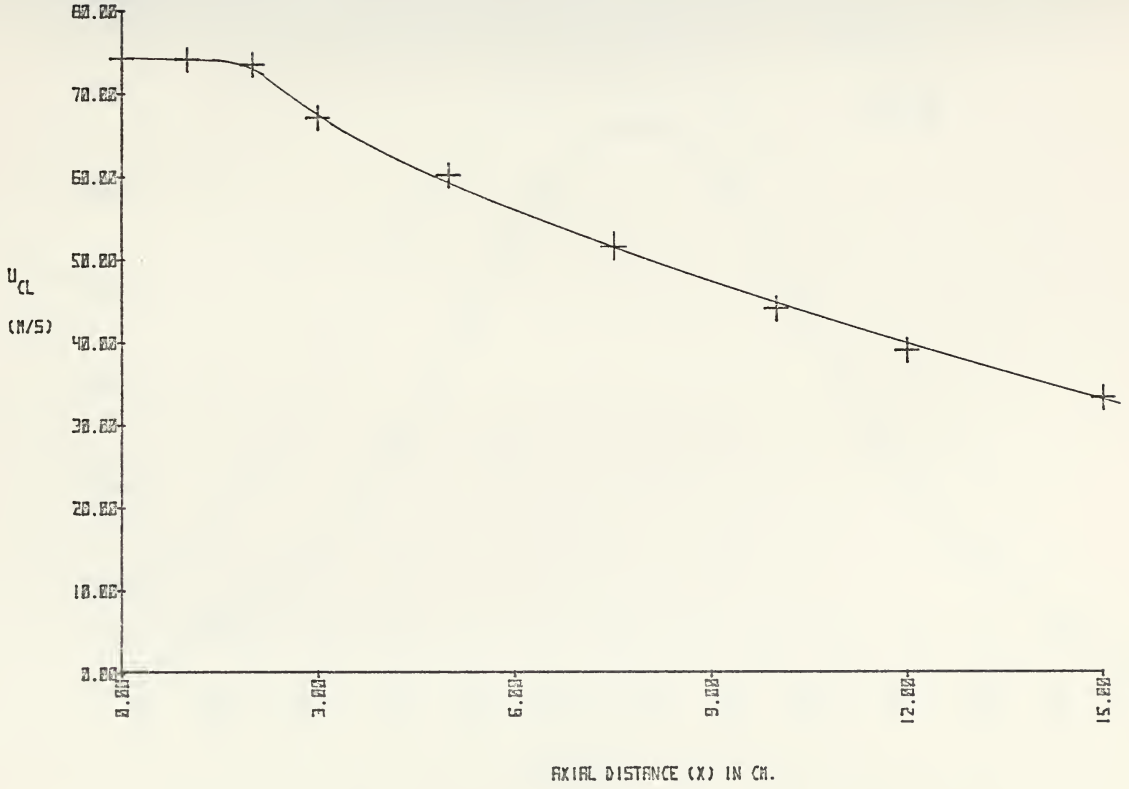

FIGURE 34. CENTERLINE VELOCITY DECAY

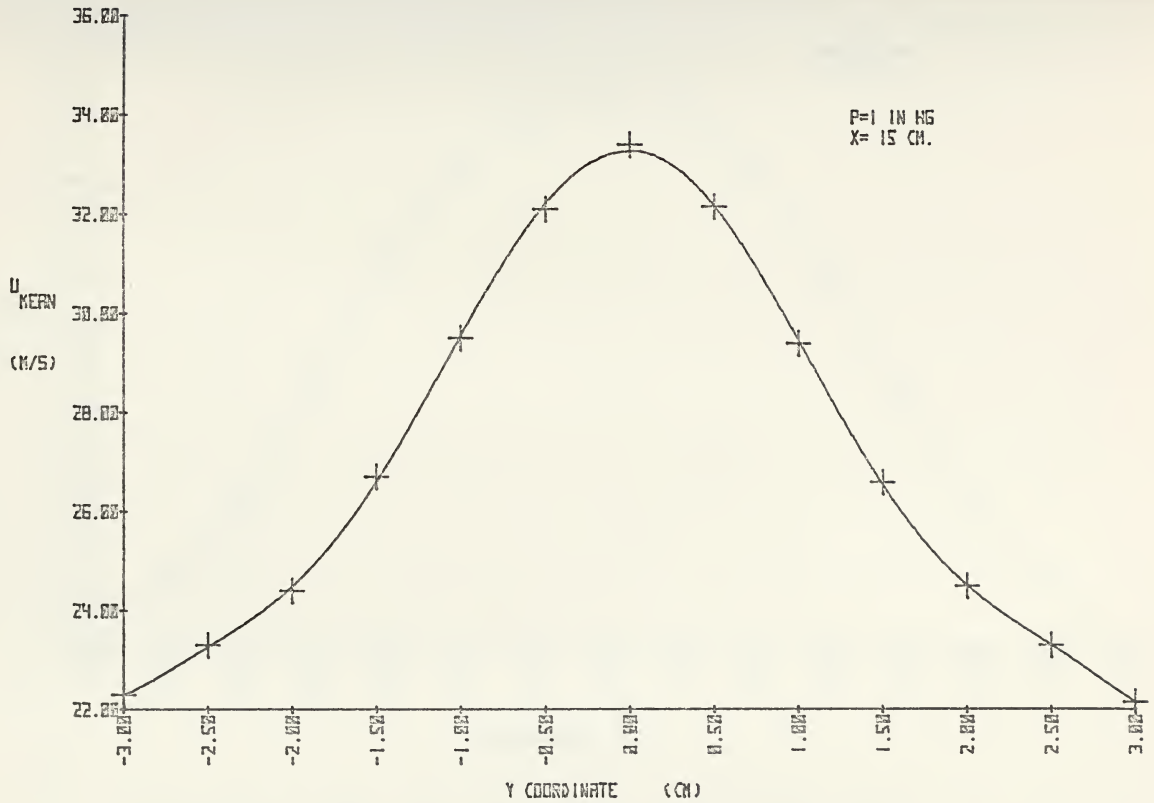

FIGURE 35. MEAN VELOCITY PROFILE OF STEADY JET

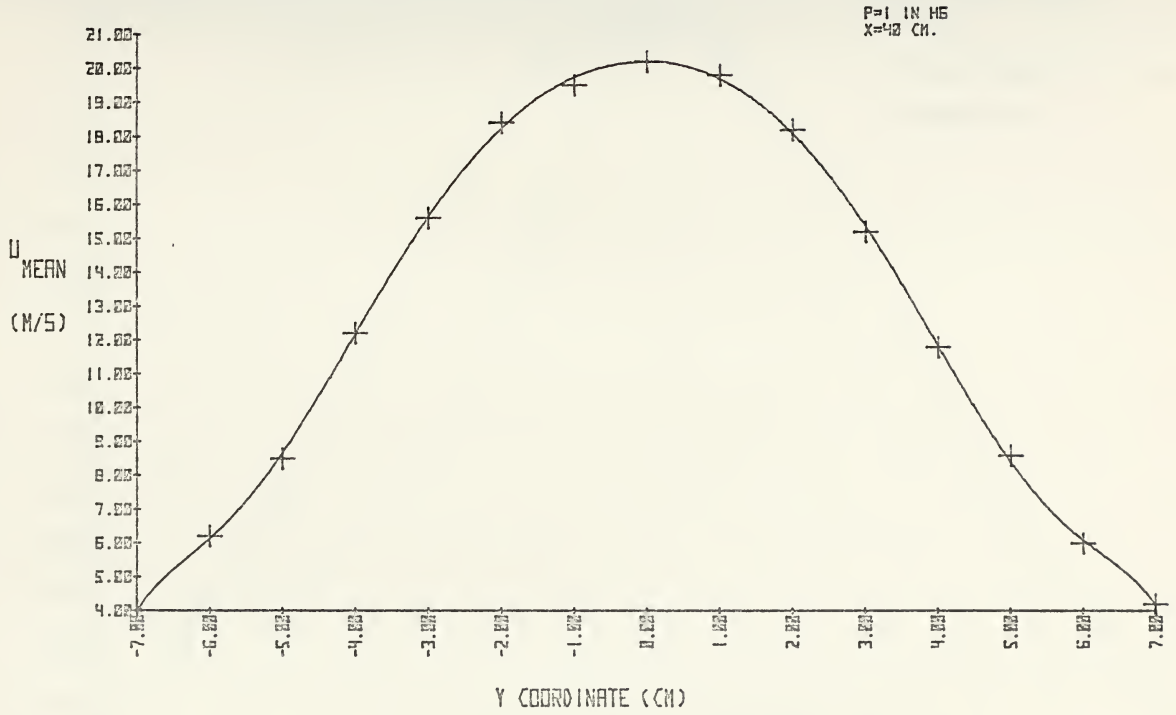

FIGURE 36. MEAN VELOCITY PROFILE OF STEADY JET

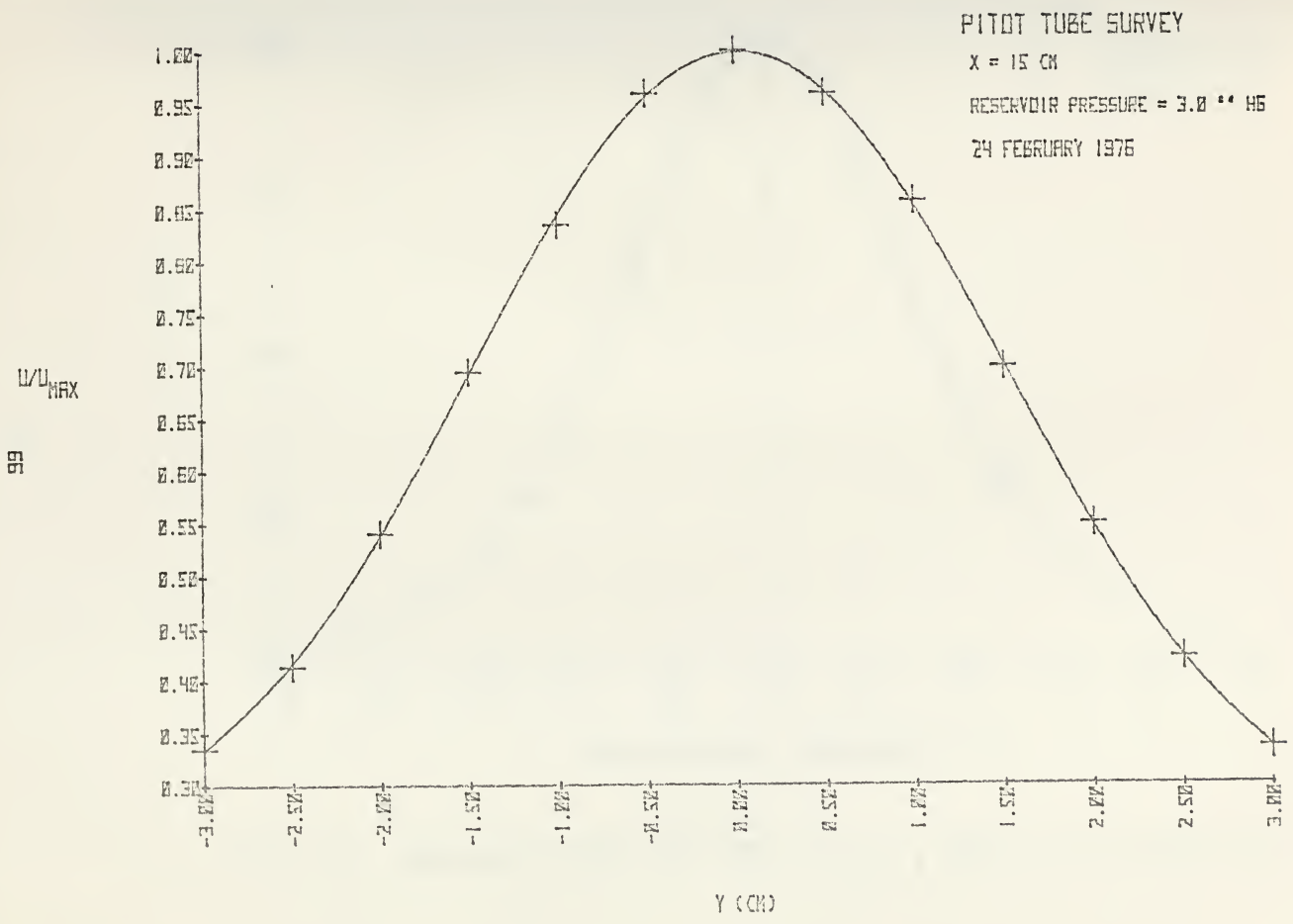

FIGURE 37. MEAN VELOCITY PROFILE OF STEADY JET

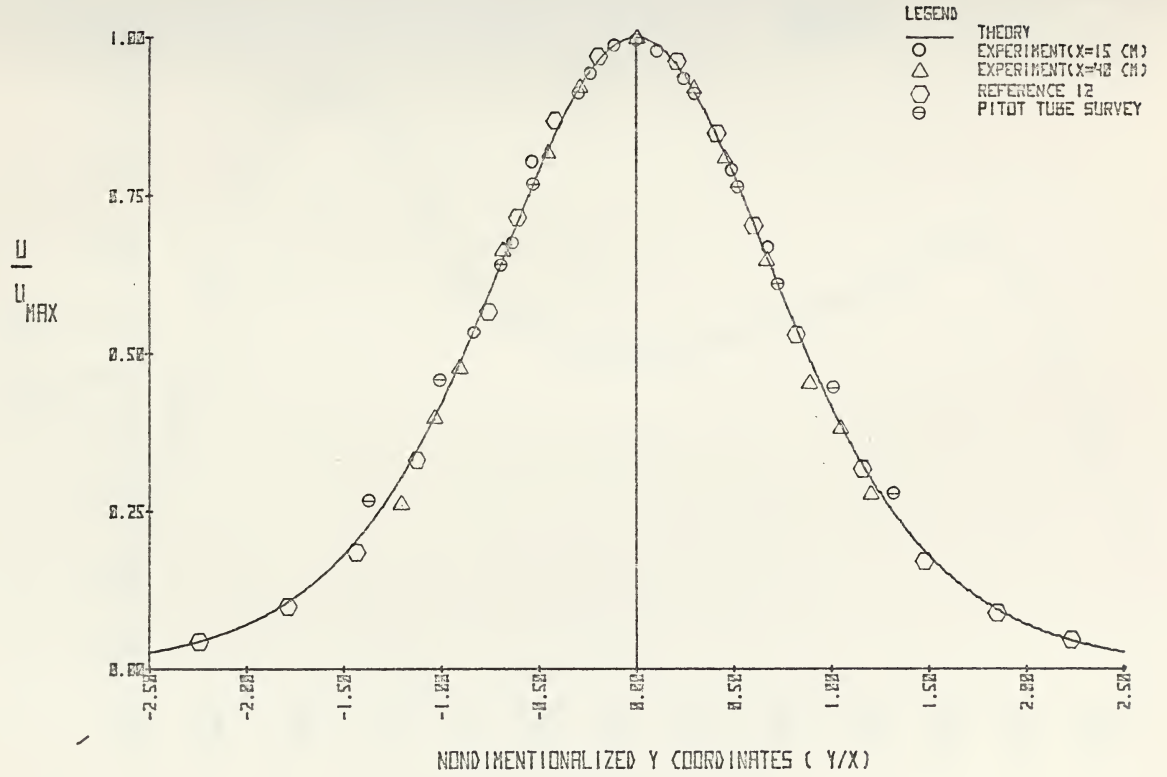

FIGURE 38. NONDIMENTIONALISED MEAN VELOCITY PROFILE OF STEADY JET

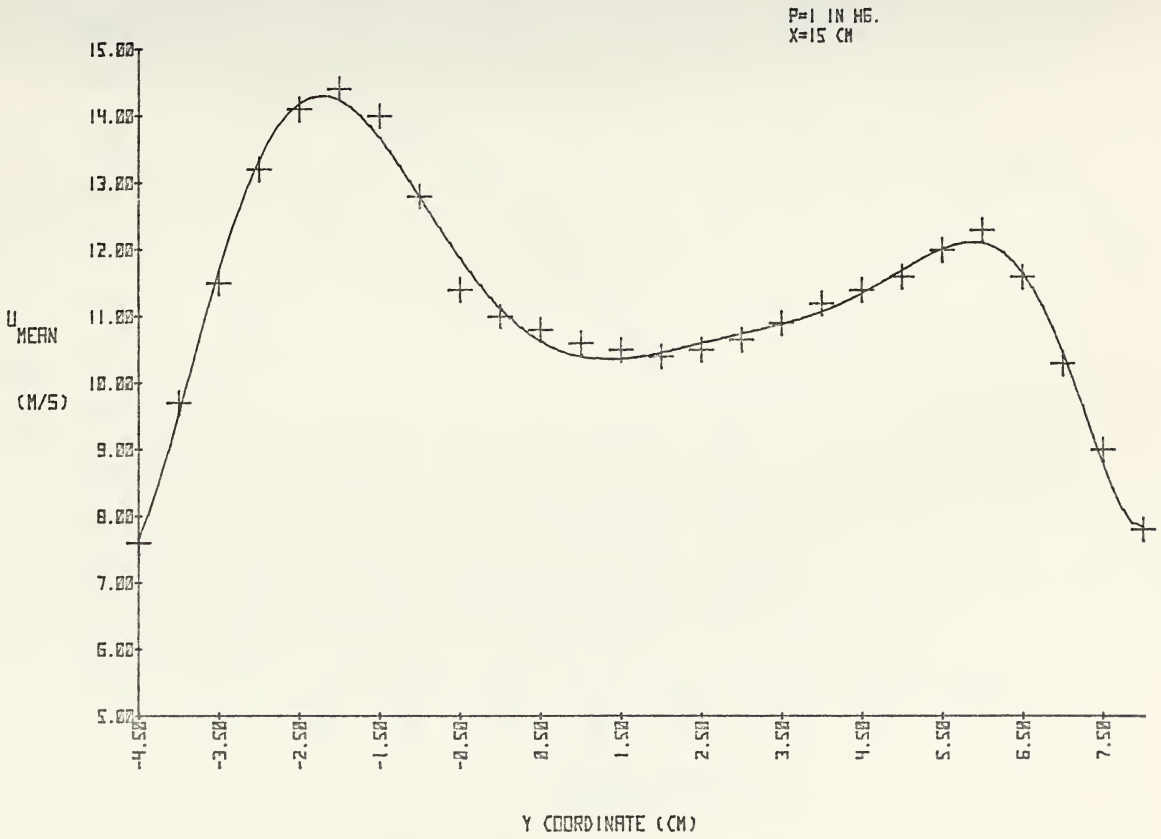

FIGURE 39. MEAN VELOCITY PROFILE OF OSCILLATING JET

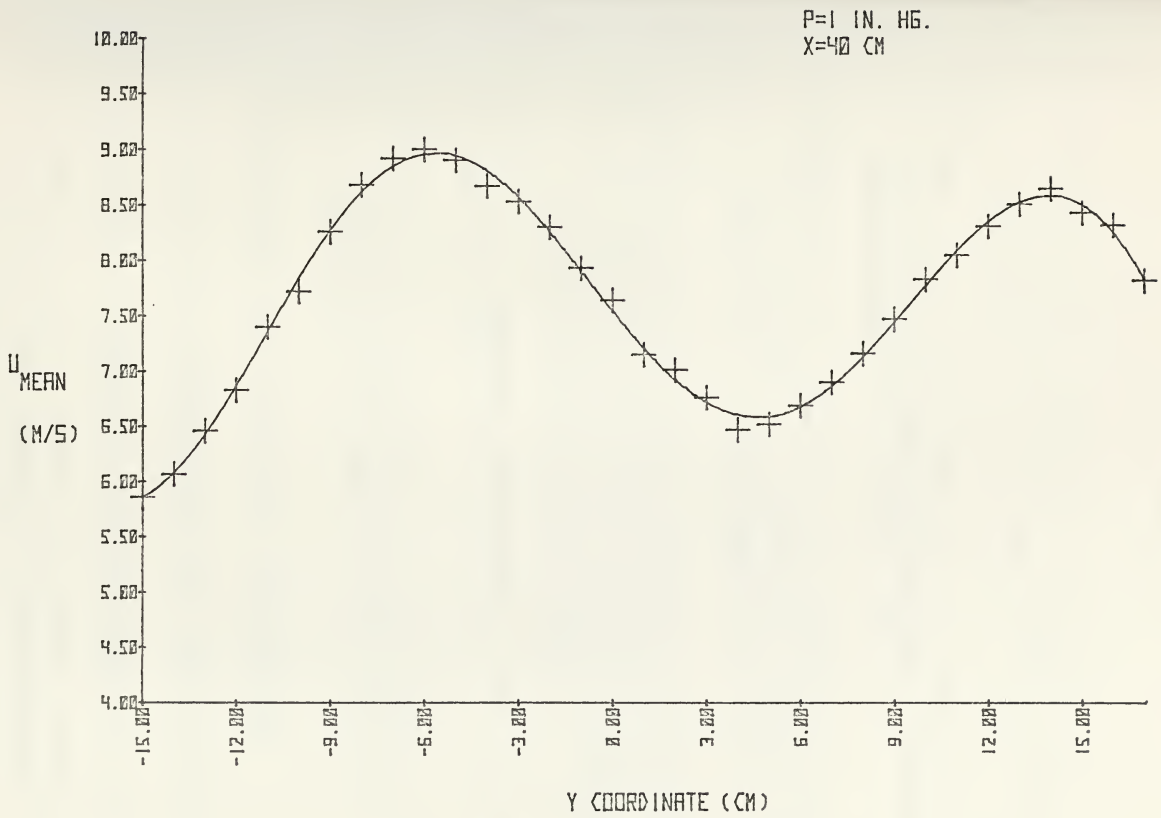

FIGURE 40. MEAN VELOCITY PROFILE OF OSCILLATING JET

LIST OF REFERENCES

1. Heflinger, L.O., Wuerker, R.R., and Brooks, R.E., 'Holography Interferometry', Journal of Applied Physics, Vol. 37, No 2. February 1966, p. 642-649

2. Chow, H.h.m., and Mullaney, G.J.,'An Example of the Application of Pulsed Light Holography to Aerodynamics, Applied Optics,Vol. 6, 1967, p. 981.

3. Rienheimer, C.J., Wiswall, C.E., Schmiege, R.A., Harris, R.J., and Decker, J.E.,'Holographic Subsonic Flow Visualization', Applied Optics, Vol 9, 1970.

4. Havener, A.G,'Holographic Application in Shadowgraph, Schlieren and Interferometry Analysis of Heat Transfer and Fluid Flow Test Subjects', Aerospace Research Laboratories Report 70-0276, Nov. 1970.

5. Smith,H.M., Principles of Holography, Wiley-Interscience, New York, 1969.

6. Hermann Viets,'Developement of a Time Dependent Nozzle', Aerospace Research Laboratories AFL TR 74-0113, August 1974.

7. Ostrovskiy, Yu.I.,'Holography', NACA TTF-706

8. Frank M. White, Viscous Fluid Flow, McGraw-Hill,Inc,1974

9. Bradshaw, P., Journal of Fluid Mechanics 26, p.1258,1966

10. Crow, S.C., and Champagne, F.H.,'Orderly Structure in Jet Turbulence', Journal of Fluid Mechanics, Vol 48, Part 3, p. 547-591, 1971.

11. Hermann Viets, Delbert Balster and Howard, L.Toms, Jr, 'Time Dependent Fuel Injectors', Wright-Patterson AFB, Ohio.

12. Pai, S.I., Fluid Dynamics of Jets, Van Nostrand Company Inc, Canada, 1954.

13. Schlichting, H., Boundary Layer Theory, 5th Edition, McGraw-Hill, New York, 1965.

14. McCormack, P.D. and Crane Lawrence, Physical Fluid Dynamics, Academic Press,New York, 1973.

15. DISA Instructional Manual.

16. Sforza, P.M., Steiger, M.H., and Trentacoste,'Studies on Three Dimensional Viscous Jets', AIAA Journal, Vol 4, 1966.

INITIAL DISTRIBUTION LIST

		No. Copies
1.	Defense Documentation Center Cameron Station Alexandria, Virginia 22314	2
2.	Library, Code 0212 Naval Postgraduate School Monterey, California 93940	2
3.	Department Chairman, Code 57 Department of Aeronautics Naval Postgraduate School Monterey, California 93940	1
4.	Professor D. J. Collins, Code 57Co Department of Aeronautics Naval Postgraduate School Monterey, California 93940	3
5.	Assoc. Professor D. W. Netzer, Code 57Nt Department of Aeronautics Naval Postgraduate School Monterey, California 93940	1
6.	Assoc. Professor M. F. Platzer, Code 57Pl Department of Aeronautics Naval Postgraduate School Monterey, California 93940	1
7.	FLT LT Ijaz A. Malik College of Aeronautical Engineering P.A.F. Base, Korangi Creek Karachi-20 Pakistan	2

Thesis 105116
M278235 Malik
c.1 Flow visualization of the turbulent jet at the exit of a single element nozzle by holographic technique, and mean velocity profile measurements with a laser Doppler anemometer.